https://doi.org/10.5194/bg-2021-337
Preprint. Discussion started: 11 January 2022

Biogeosciences Discussions Open Access EGU

High peatland methane emissions following permafrost thaw: enhanced acetoclastic methanogenesis during early successional stages

Liam Heffernan[1,2*]★, Maria A. Cavaco[3*]★, Maya P. Bhatia[3], Cristian Estop-Aragonés[4], Klaus-Holger Knorr[4], David Olefeldt[1]

[1] Department of Renewable Resources, University of Alberta, Edmonton, AB T6G 2H1, Canada. [2] Evolutionary Biology Centre, Department of Ecology and Genetics/Limnology, Uppsala University, Norbyvägen 18D, 752 36, Uppsala, Sweden. [3] Department of Earth and Atmospheric Sciences, University of Alberta, Edmonton, AB T6G 2H1, Canada. [4] Institute of Landscape Ecology, Ecohydrology and Biogeochemistry Group, University of Münster, Münster, Germany

[*]Corresponding authors: Liam Heffernan (liam.heffernan@ebc.uu.se) and Maria A. Cavaco (cavaco@ualberta.ca)

★ These authors contributed equally to this work

https://doi.org/10.5194/bg-2021-337
Preprint. Discussion started: 11 January 2022

Biogeosciences Discussions Open Access EGU

Abstract

Permafrost thaw in northern peatlands often leads to increased methane (CH_4) emissions, but gaps remain in our understanding of the underlying controls responsible for increased emissions and the duration for which they persist. We assessed how shifting ecological conditions affect microbial communities, and the magnitude and stable isotopic signature ($\delta^{13}C$) of CH_4 emissions along a thermokarst bog transect in boreal western Canada. Thermokarst bogs develop following permafrost thaw when dry, elevated peat plateaus collapse and become saturated and dominated by *Sphagnum* mosses. We differentiated between a young and a mature thermokarst bog stage (~30 and years ~200 since thaw, respectively). The young bog located along the thermokarst edge, was wetter, warmer and dominated by hydrophilic vegetation compared to the mature bog. Using 16S rRNA gene high throughput sequencing, we show that microbial communities were distinct near the surface and converged with depth, but lesser differences remained down to the lowest depth (160 cm). Microbial community analysis and $\delta^{13}C$ data from CH_4 surface emissions and dissolved gas depth profiles show that hydrogenotrophic methanogenesis was the dominant pathway at both sites. However, the young bog was found to have isotopically heavier $\delta^{13}C$-CH_4 in both dissolved gases profiles and surface CH_4 emissions, suggesting that acetoclastic methanogenesis was relatively more enhanced throughout the young bog peat profile. Furthermore, young bog CH_4 emissions were three times greater than the mature bog. Our study suggests that interactions between ecological conditions and methanogenic communities enhance CH_4 emissions in young thermokarst bogs, but these favorable conditions only persist for the initial decades after permafrost thaw.

Keywords

https://doi.org/10.5194/bg-2021-337
Preprint. Discussion started: 11 January 2022

Permafrost, peatland, thermokarst, 16S RNA, isotope, methanogenesis, microbial community, methane emissions

1. Introduction

Methane (CH_4) emissions in northern peatlands are typically thought of as being driven by environmental and ecological conditions such as temperature, water table position, and vegetation community (Bellisario et al., 1999). However, CH_4 emissions are ultimately the result of microbial activity and understanding the interactions between environmental conditions and microbial processes is key to understanding the impact of disturbances on peatland CH_4 emissions. Increased disturbances such as permafrost thaw are transforming northern latitude peatlands (Helbig, Pappas, & Sonnentag, 2016), through the disruption of the frozen and ecological conditions responsible for the regional accumulation of large peatland carbon (C) stores. Rapidly rising northern air temperatures (Mudryk et al., 2018) are predicted to lead to widespread gradual thawing of permafrost (Schaefer et al., 2011) and subsequent thermokarst development in high C density permafrost peatlands (Olefeldt et al., 2016). Thermokarst formation in ice-rich permafrost peatlands is characterized by ground subsidence and exposes previously frozen C to anaerobic microbial decomposition and potential mineralization into greenhouse gases (Schuur et al., 2015). Increased emissions of methane (CH_4) due to thermokarst formation are projected to result in a positive feedback with climate warming (Turetsky et al., 2020). However, the magnitude of peatland CH_4 emissions and the metabolic pathways responsible for these emissions in response to permafrost thaw remain uncertain, as does the period for which these conditions and emissions persist.

Methanogenesis, conducted by methanogenic archaea belonging to phylum Euryarchaeota, is one of the most prominent microbial processes contributing to the

https://doi.org/10.5194/bg-2021-337
Preprint. Discussion started: 11 January 2022

anaerobic decomposition of organic matter in water-logged permafrost soils (Cai et al., 2016; Knoblauch et al., 2018). Methanogenesis occurs primarily via two pathways: acetoclastic methanogenesis and hydrogenotrophic methanogenesis (Whiticar et al., 1986; Whiticar, 1999). Acetoclastic methanogenesis involves the cleavage of acetate into CH_4 and CO_2 and when considering these two species, causes less apparent fractionation than the hydrogenotrophic methanogenesis pathway. This results in acetoclastic methanogenesis yielding comparatively isotopically heavy $\delta^{13}C$-CH_4 ($\delta^{13}C$ = -65 to -50‰). The reduction of CO_2 and H_2 in hydrogenotrophic methanogenesis typically produces CH_4 lighter in ^{13}C ($\delta^{13}C$ = -110 to -60‰) (Hornibrook et al., 1997, 2000). While the two pathways are stoichiometrically equal (Conrad, 1999; Corbett et al., 2013), the activity of acetoclastic and hydrogenotrophic methanogens are governed by different extrinsic controls (Bridgham et al., 2013).

Acetoclastic methanogenesis accounts for two-thirds of peatland CH_4 production in northern peatlands (Conrad, 1999; Kotsyurbenko et al., 2007) and is favoured in more minerotrophic, nutrient-rich conditions, where there are sufficient levels of acetate required to fuel this pathway (Ye et al., 2012). During the initial decades following thaw, surface runoff of nutrients from surrounding intact peat plateaus (Keuper et al., 2012; 2017) and increased connectivity to regional hydrology (Connon et al., 2014), can result in more minerotrophic conditions. These shifts in hydrology, temperature, nutrients, redox conditions, and vegetation communities following permafrost thaw have been shown to increase the prevalence of acetoclastic methanogenesis and CH_4 emissions (Hodgkins et al., 2014; McCalley et al., 2014). However, this potential post-thaw enhancement of acetoclastic methanogenesis needs to be considered in context of the existing methanogenic community that developed in the peat profile before thaw. For example, historical ecological conditions have been shown to have a legacy effect on the methanogenic community following thaw and

https://doi.org/10.5194/bg-2021-337
Preprint. Discussion started: 11 January 2022

97 can therefore be a key constraint on methanogenic community structure and activity post-
98 thaw (Holm et al., 2020; Lee et al., 2012). Overall, an understanding of the methanogenic
99 community's response following thaw to shifts in both surface conditions and exposure to
100 previously frozen organic matter is key to estimating CH_4 emissions from thermokarst
101 peatlands.

102 Environmental conditions following permafrost thaw in peatlands are characterized
103 by a drastic shift in water table position and increased wetness, increased soil temperatures,
104 and a change in vegetation community associated with increased labile inputs (Beilman,
105 2001; Burd et al., 2020; Camill, 1999). These shifts may provide optimal conditions for CH_4
106 production and emissions, particularly in the initial decades following thaw. Peatland CH_4
107 emissions are constrained by the water table position (Huang et al., 2021; Strack et al., 2004),
108 and surface inundation leads to increased CH_4 emissions (Tuittila et al., 2000). Methane
109 production and emissions are positively influenced by soil temperatures (Hopple et al., 2020;
110 Olefeldt et al., 2017), and peatland CH_4 emissions have been shown to increase when both
111 the water table position and temperatures are high (Grant, 2015). The colonization of
112 vegetation associated with fresh, labile inputs has also been shown to increase both the
113 magnitude and temperature sensitivity of CH_4 emissions in peatlands (Leroy et al., 2017;
114 McNicol et al., 2020). As such, many studies have focussed on the relationship between
115 water table position, soil temperature and vegetation communities in determining CH_4 fluxes
116 following thaw (Johnston et al., 2014; Turetsky et al., 2007; Wickland et al., 2006). However,
117 while these environmental conditions are key drivers of CH_4 emissions, they are unable to
118 fully account for the variability in permafrost peatland CH_4 emissions (Juottonen et al., 2021;
119 Kuhn et al., 2021). Some of this unaccounted variance may be in part explained by microbial
120 activity, as changes in the composition and abundance of methanogenic community members
121 can contribute significantly towards peatland CH_4 emissions (Fritze et al., 2021). Relatively

https://doi.org/10.5194/bg-2021-337
Preprint. Discussion started: 11 January 2022

few studies have assessed how shifts in ecological conditions and ensuing changes in methanogenic community structure influences CH_4 emissions following thaw (McCalley et al., 2014), an interaction that may be significant both at the local and circumpolar scale.

In this study we assess the impact of permafrost thaw on peatland methanogenic community composition and CH_4 emissions along a space-for-time thaw gradient that includes an intact peat plateau and an adjacent thermokarst bog with areas that have thawed ~30 and ~200 years ago (herein referred to as young bog and mature bog, respectively). Along this gradient we assessed methanogenic community structure down to 160 cm. We hypothesize that: (1) shifting ecological conditions along the permafrost thaw gradient results in a successional microbial community and a restructuring of the methanogenic community, and (2) the warmer conditions in the young bog, along with the exposure of previously frozen peat, will result in a greater relative abundance of acetoclastic methanogens throughout the depth profile, and subsequently greater overall CH_4 emissions. In the young bog and mature bog, we measured the concentration and ^{13}C-signature of dissolved CH_4 and CO_2 down to 245 cm, and the rates and ^{13}C-signature of both CH_4 and CO_2 land-atmosphere fluxes. The combined approach of measuring dissolved gas depth profiles and surface emissions, in tandem with assessing the structure of the methanogenic community along a depth profile, allows us to determine how changing ecological conditions following thaw impacts methanogenic pathways and community composition. Utilizing this approach, we can subsequently gain further insight into how long elevated surface CH_4 emissions may persist post-thaw. Furthermore, this approach highlights that while environmental and ecological conditions are important in determining CH_4 emissions, microbial community composition, and changes in the methanogenic community structure are likely to significantly influence CH_4 emissions following thaw.

https://doi.org/10.5194/bg-2021-337
Preprint. Discussion started: 11 January 2022


Biogeosciences Discussions Open Access EGU

2. Methods

2.1 Study Site and Design

The Lutose peatland study site (59.5°N, 117.2°W; Figure 1) is located on the Interior Plains of western Canada, within the zone of discontinuous permafrost (Brown et al., 1997; Heginbottom et al., 1995). The climate is continental with a monthly average summer high temperature of 16.1 °C (July), winter low of -22.8 °C (January), and annual average air temperature of -1.8 °C (Climate-Data.org, 2019 – data from site located ~50 km south of Lutose). Annual average precipitation is 391 mm, of which three quarters fall as rain between May and September. In the discontinuous permafrost zone of the Interior Plains in boreal western Canada, ~40% of the landscape is covered by permafrost peatlands that have between 2 and 6 m deep peat deposits (Gibson et al., 2018; Vitt et al., 2000). The peatland complexes in this area are a fine-scale mosaic of permafrost peat plateaus, and permafrost-free ponds, fens, and bogs. The Lutose peatland complex is representative of the peatlands found in the discontinuous permafrost zone of the Interior Plains in western Canada. The site has 5 – 6 m deep peat and has transitioned through multiple developmental stages since it began accumulating organic matter ~8,800 years ago. It transitioned from a marsh, through a fen and a bog stage prior to permafrost aggradation ~1,800 years ago (Heffernan et al., 2020).

https://doi.org/10.5194/bg-2021-337
Preprint. Discussion started: 11 January 2022

Biogeosciences
Discussions
Open Access
EGU

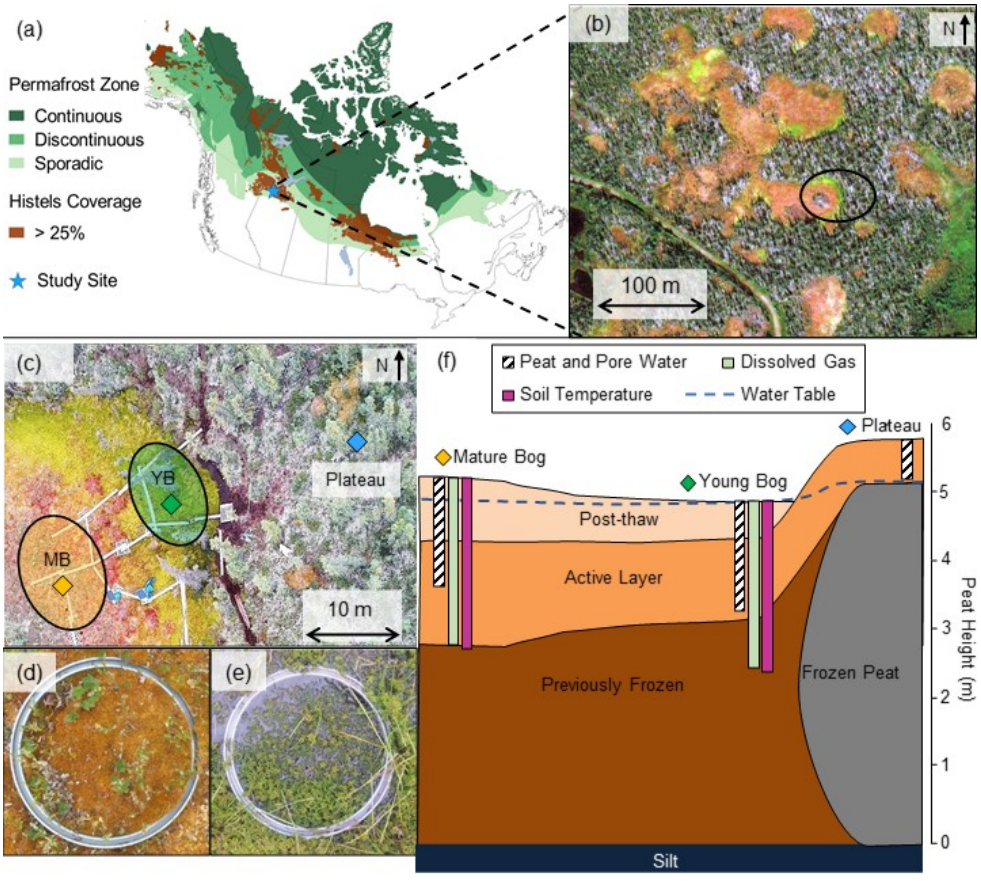

163

164 **Figure 1.** Lutose peatland site location and study design. (a) Site location (Lutose, Alberta,
165 Canada 59.5°N, 117.2°W) in boreal western Canada. Green shading represents permafrost
166 zonation (Brown et al., 1997) and brown shading represents areas with >25% permafrost
167 peatland (histels) extent (Hugelius et al., 2014). (b) Geoeye satellite image of study site
168 (image from https://zoom.earth/), 0.46 m resolution. Circle represents the area where
169 sampling took place. (c) Aerial image of study transect, locations of peat and dissolved gas
170 sampling in the plateau (blue diamond), young bog (green diamond), and mature bog (orange
171 diamond), and area where collars for gas flux measurements were located in the young bog
172 (YB, green) and mature bog (MB, orange) (Aerial photo credit: Olefeldt, David). (d, e)
173 Surface vegetation in the mature bog and young bog (f) Soil profile of thaw transect based on
174 (Heffernan et al., 2020). The transition to Post-thaw peat occurs at 29 cm and 71 cm in the
175 young bog and mature bog respectively. Peat (core) and pore water (pore water peepers),
176 including microbial community, sampling depth profile 0 – 160 cm shown as white column
177 with diagonal black lines. Dissolved gas (diffusive samplers) sampling depth profile 0 – 245
178 cm shown as light green column. Soil temperature depth profile 0 – 250 cm shown as purple
179 column. Average water table depth shown as dashed blue line.

180

https://doi.org/10.5194/bg-2021-337
Preprint. Discussion started: 11 January 2022

The studied transect represents a space-for-time gradient of permafrost thaw that includes three thaw stages: a permafrost peat plateau, and a young (~30 years since thaw) and mature (~200 years since thaw) part of an adjacent thermokarst bog. The timing of permafrost thaw was previously determined by ^{14}C dating the shift in macrofossil vegetation indicative of thaw, at 29 cm in the young bog and at 71 cm in the mature bog (Figure 1f) (Heffernan et al., 2020). The peat plateau has an active layer thickness of ~70 cm and its surface is raised 1 – 2 m above the adjacent thermokarst bog due to the presence of excess ground ice, resulting in relatively dry surface conditions where the water table generally follows the deepening of the seasonally thawed peat layer (Zoltai, 1972). This thaw stage is characterized by a stunted, open black spruce (*Picea mariana*) canopy and ground cover of lichens (*Cladonia* spp.), *Sphagnum fuscum* hummocks, and low-lying ericaceous shrubs as is characteristic of the peat plateaus in the area (Vitt et al., 1994). The young bog stage is narrow (<5 – 10 m wide) and is located next to the actively thawing area of the peat plateau. The young bog has an average growing season water table position of 1.3 ± 4.9 cm below the peat surface. These inundated conditions result in the dominance of a hydrophilic vegetation community (Figure 1e) consisting of *Sphagnum riparium*, bog-sedge (*Carex limosa*), and rannoch rush (*Scheuchzeria palustris*). The mature bog is relatively drier, compared to the young bog, with an average growing season water table position of 22.9 ± 9.3 cm below the surface. The dominant vegetation reflects these drier conditions and consists of *Sphagnum fuscum, Sphagnum magellanicum,* leather leaf (*Chamaedaphne calyculata),* cloudberry *(Rubus chamaemorus), Eriophorum vaginatum* tussocks, and some black spruce (*Picea mariana)* regrowth (Figure 1d). The mature bog is located >10 – 20 m from the thawing plateau edge.

2.2 Site Preparation and Monitoring of Environmental Conditions

https://doi.org/10.5194/bg-2021-337
Preprint. Discussion started: 11 January 2022

The Lutose peatland study site was established in 2015 and a boardwalk was constructed to minimize disturbances along the peat plateau - thermokarst bog transect. Three collars for measurements of gas fluxes (39 cm diameter) were permanently installed to a depth of 20 cm in both the young and mature bog stages. The top of each collar was aligned with the peat surface. PVC wells (2 cm diameter) were installed directly next to each collar and were used to manually monitor the water table position during each gas flux measurement. We monitored soil temperature (°C) at 10, 30, 50, 75, 100, 150, 200, and 250 cm every 30 min from May – September 2018 using permanently installed loggers (Hobo 8k Pendant Onset Computer, Bourne, MA, USA) in the young and mature bog. Temperature depth profiles were established centrally among collars in each bog stage, in areas that had similar vegetation, water table position, and distance from the thawing edge as the collars.

Custom made plexiglass pore water suction (Heffernan et al., 2021) and diffusive equilibration gas sampling devices (Knorr et al., 2009) were installed in July 2016 in the young bog and mature bog. These devices were installed in the young and mature bog stages, ~1 m from the nearest collar. Pore water suction devices were installed to a depth of 160 cm deep and consisted of 15 sampling depths connected to the surface via silicone tubing. This allowed for repeated non-destructive pore water sampling. Three diffusive gas sampling devices each were installed in the young and mature bog, where two collected dissolved soil gas samples from 5 – 95 cm deep and the third from 115 – 245 cm. Each sampler consisted of a PVC pipe with a 10 cm sampling section centred at each sampling depth. Sampling sections consisted of ~2 m of silicon tubing (3 mm i.d., 5 mm o.d.) wrapped around the PVC pipe and kept in place by PVC-spacers at the top and bottom of each interval. Silicone tubes were sealed at one end whereas the other end was connected to polyurethane tubing (1.8 mm i.d.) that ran back up inside the PVC tube to reach the peat surface where it was sealed with a three-way stopcock. Silicone tubing has been shown to be permeable to gases such as CO_2

https://doi.org/10.5194/bg-2021-337
Preprint. Discussion started: 11 January 2022

and CH_4 within a number of hours, while remaining impermeable to water, making it suitable for sampling of dissolved soil gases (Kammann et al., 2001).

2.3 Pore water chemistry and peat enzyme activity

Pore water dissolved organic matter (DOM) chemistry and peat enzyme activity presented in this study have previously been published (Heffernan et al., 2021), and are briefly described here. Pore water samples for DOM chemistry were taken monthly from May – September 2018 using the previously described pore water suction devices in the young bog and mature bog. Three 60 mL samples were taken from all 15 measurement depths by applying a vacuum at the surface and collecting water with syringes via a three-way stopcock. Each water sample was immediately filtered through 0.7 µm pore size glass fiber filters (GF/F Whatman) into two acid-washed amber glass bottles, with one sample acidified with 0.6 mL 2N HCl to prevent further microbial activity. Pore water samples were transported in a cooled container and stored at 4 °C prior to analysis. Pore water DOM was analyzed for pH, phosphate (PO_4^{3-}; µg L^{-1}), dissolved organic carbon (DOC; mg L^{-1}), total dissolved nitrogen (TDN; mg L^{-1}) concentrations, phenolic contents, specific UV absorbance at 254 nm (SUVA, L mg C^{-1} m^{-1}; Weishaar et al., 2003) and spectral slope between 250 – 465 nm ($S_{250-465}$, nm^{-1}; Helms et al., 2008). SUVA and $S_{250-465}$ values are used to indicate aromaticity, with high SUVA indicating a high aromatic content and lower $S_{250-465}$ indicating low molecular weight and decreasing aromaticity (Hansen et al., 2016).

Peat cores extracted to a depth of 160 cm were stored at 4 °C for less than one week in the laboratory before homogenization to determine potential soil enzyme activities. We performed hydrolytic enzyme assays for four enzymes; phosphatase, β-N-glucosaminidas, β-glucosidase, and β-cellobiosidase using fluorogenic 4-methylumbelliferone labelled substrates (Dunn et al., 2014). We assayed oxidative enzyme activity by measuring laccase

https://doi.org/10.5194/bg-2021-337
Preprint. Discussion started: 11 January 2022

activity using syringaldazine (Criquet et al., 2000; Jassey et al., 2012). We summarized the activity of all enzymes using a multi-functionality index based on *z*-scores (Allan et al., 2015; Heffernan et al., 2021).

2.4 Surface Land-Atmosphere Gas Fluxes

We measured surface land-atmosphere greenhouse gas fluxes (CH_4 and carbon dioxide; CO_2) monthly from May – September 2018 at the 3 collars in each peatland stage using the static chamber method (Carroll & Crill, 1997). The chamber used to capture land-atmosphere fluxes was a transparent cylindrical Plexiglass chamber with a basal area of 0.12 m^2, height of 0.40 m, and volume of 47.8 L. The chamber was equipped with three fans (Micronel Ventilator D341T012GK-2, BEDEK GmbH, Dinkelsbühl, Germany) to mix air during measurements and a temperature sensor (Hobo RH Smart Sensor, S-THB-M002, Onset computers, Bourne, USA) that was shaded from direct sunlight (Burger et al., 2016). An airtight seal was formed between the chamber and collar by pouring water in a ~1.5 cm deep well around the upper circumference of each collar. Land-atmosphere fluxes of CO_2 (ecosystem respiration) and CH_4 were captured simultaneously in darkened conditions by covering the chamber with a reflective shroud. Gas concentrations were determined at a temporal resolution of 1 s using an Ultraportable Greenhouse Gas Analyser (Los Gatos Research, CA, USA) and real-time fluxes were monitored using the VNV® Viewer (RealVNC® Limited, UK) application with an iPad mini 2 (Apple Inc.).

The rates of CH_4 and CO_2 land-atmosphere fluxes were calculated using the change in gas concentration over time inside the chamber (linear regression), the ideal gas law, average air temperature inside the chamber during the measurement, and a constant atmospheric pressure value of 0.96 atm in Eq. (1):

$$Flux = slope \frac{P.V}{R.T.A} \quad (1)$$

https://doi.org/10.5194/bg-2021-337
Preprint. Discussion started: 11 January 2022

Slope is the linear rate of change of gas concentration (μmol mol^{-1} $second^{-1}$) over the measurement period inside the chamber; P is atmospheric pressure (atm); V is chamber volume (L); R is the universal gas constant (L atm K^{-1} mol^{-1}); T is the temperature (K); and A is the chamber basal area (m^2). Chamber closure for each flux measurement was 5 minutes with the first 2 minutes discarded to ensure fluxes (i.e., change in concentration over time) with $R^2 > 0.75$. We report CO_2 fluxes in g CO_2 m^{-2} day^{-1} and CH_4 fluxes in mg CH_4 m^{-2} day^{-1}, with positive values indicating fluxes to the atmosphere. To quantify the proportion of C being emitted as CH_4 we standardized our CO_2 and CH_4 fluxes per g C emitted. The proportion of C emitted as CH_4 was calculated as CH_4:C emissions = g C-CH_4 m^{-2} day^{-1}/(g C-CO_2 m^{-2} day^{-1} + g C-CH_4 m^{-2} day^{-1}).

2.5 ^{13}C-signature of CH_4 emissions

We assessed the ^{13}C-CO_2 and ^{13}C-CH_4 signatures of ecosystem respiration (CO_2) and CH_4 emissions. This was done similarly to regular measurements of CO_2 and CH_4 fluxes, but using a smaller, opaque chamber of 31.1 L and discrete syringe-samples for ^{13}C analysis in combination with the continuous monitoring of gas concentrations described above. Gas syringe samples were taken using a 20 mL syringe via a three-way stopcock placed between the sealed chamber and gas inlet port on the Ultraportable Greenhouse Gas Analyser. Gas samples were then injected into a 37.5 mL sealed glass-vial that had been flushed with nitrogen gas prior to sealing. Chamber enclosure time ranged from 30 – 50 minutes with 4 – 5 samples being taken during this time. Samples were taken either every 10-minutes or once a minimum change in CO_2 (30 μmol mol^{-1}) and CH_4 (1 μmol mol^{-1}) concentrations was observed. An atmospheric gas sample was used as a time-zero measurement when assessing the change in concentration over time. Glass-vials containing samples were stored at 4 °C

https://doi.org/10.5194/bg-2021-337
Preprint. Discussion started: 11 January 2022

until analysis. These measurements were taken in September and October 2016 from 1 collar in both the young and mature bog, with each collar measured twice.

Gas vials containing both the chamber and atmospheric gas samples were analysed in the laboratory for ^{13}C isotopic signatures. Concentrations of CO_2 and CH_4, using between 1 – 3 mL from each vial, were checked in order to validate the tightness of the containers and to ensured that concentrations fit within the measurement range required for ^{13}C analysis. Subsequently, after measurement of the concentration of CO_2 and CH_4 in each sample, the ^{13}C-CO_2 and ^{13}C-CH_4 signature was quantified in-line with a cavity ring-down spectrometer (G2201-L, Picarro, California, USA) that had been calibrated using certified standards. To this end, the remaining sample (17 – 19 ml) was diluted with nitrogen gas to a final volume of 20 mL and injected for analysis into a Small Sample Introduction Module (SSIM, Picarro, California, USA) system to measure ^{13}C signatures.

We then used the time-series of ^{13}C-CH_4 and CH_4 concentrations to estimate the ^{13}C-CH_4 signature of the CH_4 released to the atmosphere using Keeling plots (Keeling, 1958). Using this approach, the ^{13}C-CH_4 signature of gas in each sample is plotted on the *y*-axis against the inverse of CH_4 gas concentrations ($1/CH_4$). The *y*-axis intercept of the linear regression represents the mean isotopic signature of the CH_4 source (Fisher et al., 2017). While fractionation during diffusive transport may influence these estimates, it has been shown in similar systems to be of minor importance compared to other contributing processes (Preuss et al., 2013; Nielsen et al., 2019).

2.6 Dissolved gas depth profiles

Dissolved gas samples were taken using the diffusive equilibration gas sampling devices. Samples were taken from 15 depths that include 5 – 15 cm and then every 10 cm down to 95 cm, and then at 115 cm, 140 cm, 165 cm, 195 cm, and 245 cm. Samples of ~7 mL were drawn from each depth monthly from May – September in 2018 using 10 mL plastic

https://doi.org/10.5194/bg-2021-337
Preprint. Discussion started: 11 January 2022

syringes. Samples were immediately injected into a 10 mL sealed glass-vial that had been flushed with nitrogen gas prior to sealing. Glass-vials containing samples were stored at 4 °C until analysis. Concentrations of dissolved CO_2 and CH_4 for each were analysed using a gas chromatograph with an FID and CO_2 methanizer (8610C Gas Chromatograph, SRI Instruments, California, USA) for a total of 214 and 211 concentrations of CO_2 and CH_4, respectively. Between 1 – 3 mL of gas was injected into the analyser. Signatures of $^{13}C\text{-}CO_2$ and $^{13}C\text{-}CH_4$ were measured with the previously mentioned method using the cavity ringdown spectrometer and SSIM system. As with surface gas samples, dissolved gas samples were diluted with N_2 to 20 ml. However, dissolved gas concentrations were considerably higher than gas concentrations found in the surface chambers, and some were well above the range concentration required for accurate ^{13}C analysis for the SSIM system even after dilution. Due to the optimal operational range of the SSIM system used, further dilution of samples to CH_4 concentrations within the systems measurable range resulted in CO_2 concentrations below detectable limits. As such, we were able to obtain 90 and 75 measurements of $^{13}C\text{-}CH_4$ in the young and mature bog, respectively, and 93 measurements of $^{13}C\text{-}CO_2$ in both.

We used the $^{13}C\text{-}CO_2$ and $^{13}C\text{-}CH_4$ signature of each gas sample to calculate the apparent fraction factor α_c, where $\alpha_c = [^{13}C\text{-}CO_2 + 1000]/[^{13}C\text{-}CH_4 + 1000]$. The α_c can serve as an isotopic indicator of the pathway of methanogenesis, with typical values of 1.060 – 1.090 observed for hydrogenotrophic methanogenesis and 1.040 – 1.060 for acetoclastic methanogenesis (Chanton et al., 2005).

2.7 Peat and pore water sample collection for microbial community composition analyses

https://doi.org/10.5194/bg-2021-337
Preprint. Discussion started: 11 January 2022

348 Microbial community composition was characterized in both peat and peat pore water
349 samples from depths between 0 – 160 cm in the young bog and mature bog. Focussing on
350 peat samples, microbial community composition in the active layer of the peat plateau was
351 assessed from depths between 0 – 30 cm. Peat cores were extracted in June and September
352 2018. Near-surface cores were extracted using a cutting tool to 30 cm deep in the peat plateau
353 and young bog, and 50 cm deep in the mature bog. Surface cores were limited to 30 cm in the
354 plateau due to the presence of ground ice during sampling in June. Surface core depths
355 differed between the young bog and mature bog due to differences in the water table position.
356 Deeper core sections (down to 160 cm) in the young bog and mature bog were extracted
357 using a Russian peat corer (4.5 cm inner-diameter, Eijkelkamp, Giesbeek, The Netherlands).
358 Cores were extracted from two boreholes located ~20 cm apart, alternating between
359 boreholes to avoid disturbance contamination from the 10 cm corer tip during the coring
360 process. To do so, 50 cm long core sections were taken alternatively from each borehole, with
361 each core having a 10 cm overlap with the previous core taken from the adjacent borehole. In
362 the field, immediately after the entire core was extracted, cores were divided into 15
363 subsections. The first two subsections contained peat from 0 – 5 cm and 5 – 10 cm, followed
364 by 10 cm increments down to 120 cm, and two further subsections from 130 – 140 cm and
365 150 – 160 cm. Peat from each interval was sub-sampled using sterilized forceps and placed
366 directly into Whirl-Pak® bags, and frozen within 3 hours of sampling for transportation back
367 to the laboratory. Once samples reached the laboratory, they were frozen at -80 °C until
368 analysis.

369 We also sampled peat pore water at all 15 peat sampling depths in September 2018 from
370 the pre-installed pore water suction sampling devices mentioned above. We extracted 60 mL
371 pore water samples by applying a vacuum at the surface and collecting water with new plastic
372 60 mL syringes. Pore water was immediately filtered through sterile 0.2 µM pore size PVDF

https://doi.org/10.5194/bg-2021-337
Preprint. Discussion started: 11 January 2022

membrane sterivex filters (MilliporeSigmna). Microbial cells were retained on the filter, and remaining porewater in the sterivex was removed via extrusion using a 60 mL sterile syringe. Sterivex filters were then immediately flash-frozen at -80 °C in a liquid nitrogen dry-shipper to preserve microbial community members until analysis could take place.

2.8 DNA extraction

Microbial DNA was extracted from all peat and pore water samples using the DNeasy PowerSoil kit (Qiagen) and the PowerWater DNeasy kit (Qiagen), respectively, to assess the differences in microbial community structure. Extraction of DNA from both sample types was followed as described by the manufacturer (Qiagen), with two modifications: (i) for peat samples, prior to mechanical lysis using bead beating, the prepared samples were chemically lysed by incubation at 70 °C for 10 minutes in the provided lysis solution, and (ii) sterivex (pore water) samples were incubated with rotation at 37 °C following addition of lysis buffer. These modifications were made to increase total DNA yield. The amount of isolated DNA from each sample was then determined using a Qubit fluorometer (model 2.0, using the 1×HS dsDNA kit), with concentrations ranging between ~0.1 and 22.4 ng μL^{-1}. This extracted DNA served as the template for polymerase chain reaction (PCR) analyses described below.

2.9 *Sequencing and computational analyses*

We amplified 16S rRNA genes using universal prokaryotic primers 515F (Parada, Needham & Fuhrman, 2016) and 926R (Quince et al., 2011). Each primer also contained a six-base index sequence for sample multiplexing (Bartram et al., 2011). The PCR mix (25µL total volume) contained 1 × Q5 reaction buffer, 0.5 µM forward primer, 0.5 µM reverse primer, 200 µM dNTPs, 0.500 U Q5 polymerase (New England Biolabs, Ipswich,M.A, U.S.A) and 2.5 µL of genomic template. Genomic extracts with DNA concentrations of greater than 2 ng μL^{-1} were diluted 1:100 in nuclease-free water. The PCR was performed as follows: 95 °C for 3 minutes, 35 cycles of 95 °C for 30 seconds, 60 °C for 30 seconds, 70 °C

https://doi.org/10.5194/bg-2021-337
Preprint. Discussion started: 11 January 2022

for 1 minute and a final extension of 70 °C for 10 minutes. Pooled 16S rRNA gene amplicons were purified using Nucleomag beads and a 4.5 pM library containing 50% PhiX Control v3 (Illumina, Canada Inc., NB, Canada) was sequenced on a MiSeq instrument (Illumina Inc., CA, USA) using a 2 × 250 cycle MiSeq Reagent Kit v3 (Illumina Canada Inc) at the Molecular Biology Service Unit (MBSU, University of Alberta). The MiSeq reads were demultiplexed using MiSeq Reporter software version 2.5.0.5. Each read pair was assembled using the paired-end assembler for Illumina sequences (PANDAseq; Masella, Bartram & Truszkowski, 2012) with a quality threshold of 0.9, dictating that 90% of overlapping reverse and forward reads must match in order to assemble reads into read pairs. Assembled reads were analyzed using the Quantitative Insights Into Microbial Ecology II pipeline (QIIME2; Boylen et al., 2020). Sequences were clustered into amplicon sequence variants (ASVs) with chimeric sequences, singletons and low abundance ASVs removed using DADA2 (Callahan et al., 2019). All representative sequences were classified with the Greengenes reference database, using the most recent release (version 13.8; McDonald et al., 2012).

2.10 Statistics

All statistical analyses were carried out in R (Version 3.4.4, R Core Team, 2015) using the *nlme*, *vegan*, *factoextra*, *ggplot2*, *VariancePartition* and *ggpubr* packages (Pinheiro et al., 2017; Oksanen et al., 2013; Kassambara & Mundt, 2017; Wickham, 2016; Hoffman & Schadt, 2016; Kassambara, 2018). For Analysis of Variance (ANOVAs), distribution of the data was inspected visually for normality along with the Shapiro-Wilk test. We tested homogeneity of variances using the *car* package and Levene's test (Fox and Weisberg, 2011). We report uncertainty as ± 1 standard deviation, except for land-atmosphere greenhouse gas fluxes which we report as ± 95% confidence intervals. We here define the statistical significance level at 5%.

https://doi.org/10.5194/bg-2021-337
Preprint. Discussion started: 11 January 2022

We used ANOVAs and Bonferroni post-hoc tests on linear mixed effects models to evaluate significant differences and seasonal trends in greenhouse gas fluxes and dissolved gas depth profiles. These were performed with a focus on assessing whether thaw stage (young bog or mature bog) influenced greenhouse gas fluxes and dissolved gas depth profiles. This approach was used to test for significant differences in CH_4 fluxes, ratio of CH_4:C emissions, and source ^{13}C-CH_4 signature intercepts of Keeling plots between young bog and mature bog stages. In each linear mixed effect model, sampling month and peatland stage were defined as fixed effects whereas sampling collar was defined as a random effect. Similarly, we assessed for significant differences in depth profiles of dissolved CH_4 and CO_2 concentrations, $\delta^{13}C$-CH_4 and $\delta^{13}C$-CO_2 signatures, and α_c between the young bog and mature bog. In these models, sampling month and peatland stage were defined as fixed effects while sample depth was defined as a random effect.

Following microbial 16S rRNA gene sequencing on an Illumina Miseq, sample reads were rarefied to the lowest read count of 28,129 for all subsequent analyses. These sequences represent whole microbial community data that was used to determine whether there was evidence of changes in microbial community structure representing the successional peatland stages following permafrost thaw throughout the 160 cm depth peat profile. In addition, we assessed differences in community composition across both peat and pore water and to determine whether seasonality impacted microbial community structure in both sample matrices. Here, Bray Curtis dissimilarity matrices for overall microbial community data were used, at 999 permutations, to identify distinct groupings assessed at the 95% confidence interval in NMDS ordinations. These distinct groupings were further evaluated for significance using the non-parametric Analysis of Similarities (ANOSIM) test.

Methanogens were selected at the order level from our whole community data using Greengenes-assigned taxonomy. Utilizing their assigned taxonomy, the pathways through

https://doi.org/10.5194/bg-2021-337
Preprint. Discussion started: 11 January 2022

447 which identified methanogens conduct methanogenesis was determined by comparing our
448 findings with the literature (Berghuis et al., 2019; Stams et al, 2019). Focusing on the
449 methanogenic community allowed us to specifically assess how permafrost thaw affects the
450 microbial community responsible for CH_4 production and net CH_4 emissions following thaw.
451 We utilized our methanogenic community data to construct redundancy analyses (RDA) and
452 relative abundance bar plots. RDAs were conducted using a Hellinger-transformed
453 methanogenic community. Explanatory variables (i.e., dissolved concentrations of CO_2, CH_4,
454 DOC, temperature, enzymatic activity estimate, thaw stage, depth, and distance to water
455 table) were scaled about the mean. These explanatory variables had variance standardized,
456 were checked for collinearity (parameters with variance inflation value > 10 were removed)
457 and selected for significance using backward selection, set at 1,000 permutations. The
458 significance of the RDA model, and of each axis was tested using ANOVAs, set at 999
459 permutations. Variance partitioning analyses were conducted to assess the contribution of
460 significant environmental parameters (i.e., thaw stage and distance to water table) on the
461 structuring of the Hellinger-transformed methanogenic community. Distance from water table
462 reflects the distance (in cm) a certain sample is from the water table in different stages of
463 thaw (young bog and mature bog). Due to the smaller size of our methanogenic community
464 relative to the total community, and the lack of some data at certain depths, we combined
465 pore water and peat samples together for these analyses. Relative abundance, which measures
466 how common or rare a particular microorganism is relative to others in the entire microbial
467 community, of methanogenic orders related to acetoclastic or hydrogenotrophic
468 methanogenesis processes were plotted according to depth. Significant differences in
469 methanogenic community composition between depths were assessed using the non-
470 parametric Kruskall-Wallis test with a Benjamini-Hochberg correction for multiple
471 comparisons, after running a Wilcox rank sum test.

https://doi.org/10.5194/bg-2021-337
Preprint. Discussion started: 11 January 2022

3. Results

3.1 Site environmental conditions

The young bog was wetter and warmer than the mature bog throughout the May – September 2018 study period. In June, following snowmelt, the water table was at its highest at 2.2 ± 0.6 cm above the surface in the young bog. The highest water table position in the mature bog was 17.5 ± 1.9 cm below the peat surface and observed in July. The water table dropped during the season and in September was 5.7 ± 2.2 cm and 27.3 ± 1.2 cm below the peat surface, in the young bog and mature bog respectively. In the plateau, the seasonally thawed layer gradually deepened during the growing season, with an active layer depth of 79.5 ± 13.7 cm measured in September. The water table in the peat plateau followed the deepening of the seasonally thawed layer.

Soil temperatures followed the seasonal climate but were dampened and had temporal lags in deeper peat layers (Figure S1a). The highest young bog and mature bog soil temperatures at 10 cm depth occurred in July, at 14.3 and 14.1 °C, respectively. At 100 cm depth the maximum temperatures occurred in August and September, at 8.6 and 6.9 °C, respectively for the young and mature bog. Soil temperatures at 250 cm were still rising at the end of September, peaking at 4.1 and 3.2 °C in the young bog and mature, respectively. The young bog was consistently warmer than the mature bog throughout the study by on average 0.9 ± 0.9 °C, 1.8 ± 1.0 °C, and 0.5 ± 0.4 °C at 10 cm, 100 cm, and 250 cm depths, respectively.

Across all depths and sampling occasions, average pH was higher in the young bog than in the mature bog at 4.1 ± 0.2 and 3.9 ± 0.2 respectively. Average SUVA was also higher in the young bog (3.2 ± 0.4 L mg C^{-1} m^{-1}) compared to the mature bog (2.6 ± 0.4 L mg C^{-1} m^{-1}), indicating DOM with a greater aromatic content in the young bog. In contrast, DOC

https://doi.org/10.5194/bg-2021-337
Preprint. Discussion started: 11 January 2022

(69.2 ± 18.4 and 53.8 ± 5.4 mg C L^{-1}) and total dissolved nitrogen (1.5 ± 1.4 and 0.9 ± 0.1 mg L^{-1}) were higher in the mature bog than in the young bog, respectively. Average phenolics (0.6 ± 0.2 and 0.6 ± 0.2 mg L^{-1}), spectral slope ($S_{250-465}$: -0.016 ± 0.002 and -0.017 ± 0.003 nm^{-1}), and phosphate (PO_4^{3-}: 9.0 ± 14.3 and 6.7± 3.0 µg L^{-1}) were similar between the young bog and mature bog, respectively, across all depths and sampling occasions. Full details of DOM chemistry results can be found in Heffernan et al., (2021).

3.2 Concentrations and isotopic signatures of dissolved gases

Dissolved CH_4 increased with depth under the water table in both the young and mature bog (Figure 2a). Concentrations of CH_4 in the young bog increased with depth, from 19 µmol L^{-1} at 5 cm depth, to a peak of 5,400 µmol L^{-1} at 195 cm. Concentrations of CH_4 in the mature bog remained low above the water table (<6 µmol L^{-1} below 25 cm), but then increased to 4,100 ± 1,700 µmol L^{-1} between 115 and 250 cm depth. Dissolved CO_2 concentrations followed a very similar pattern to CH_4, increasing with depth in both the young and mature bog (Figure 2b). Again, the mature bog had overall higher concentrations, peaking at 1,500 µmol L^{-1} at 85 cm while the young bog peaked at 1,200 µmol L^{-1} at 95 cm (Figure 2b).

https://doi.org/10.5194/bg-2021-337
Preprint. Discussion started: 11 January 2022

512

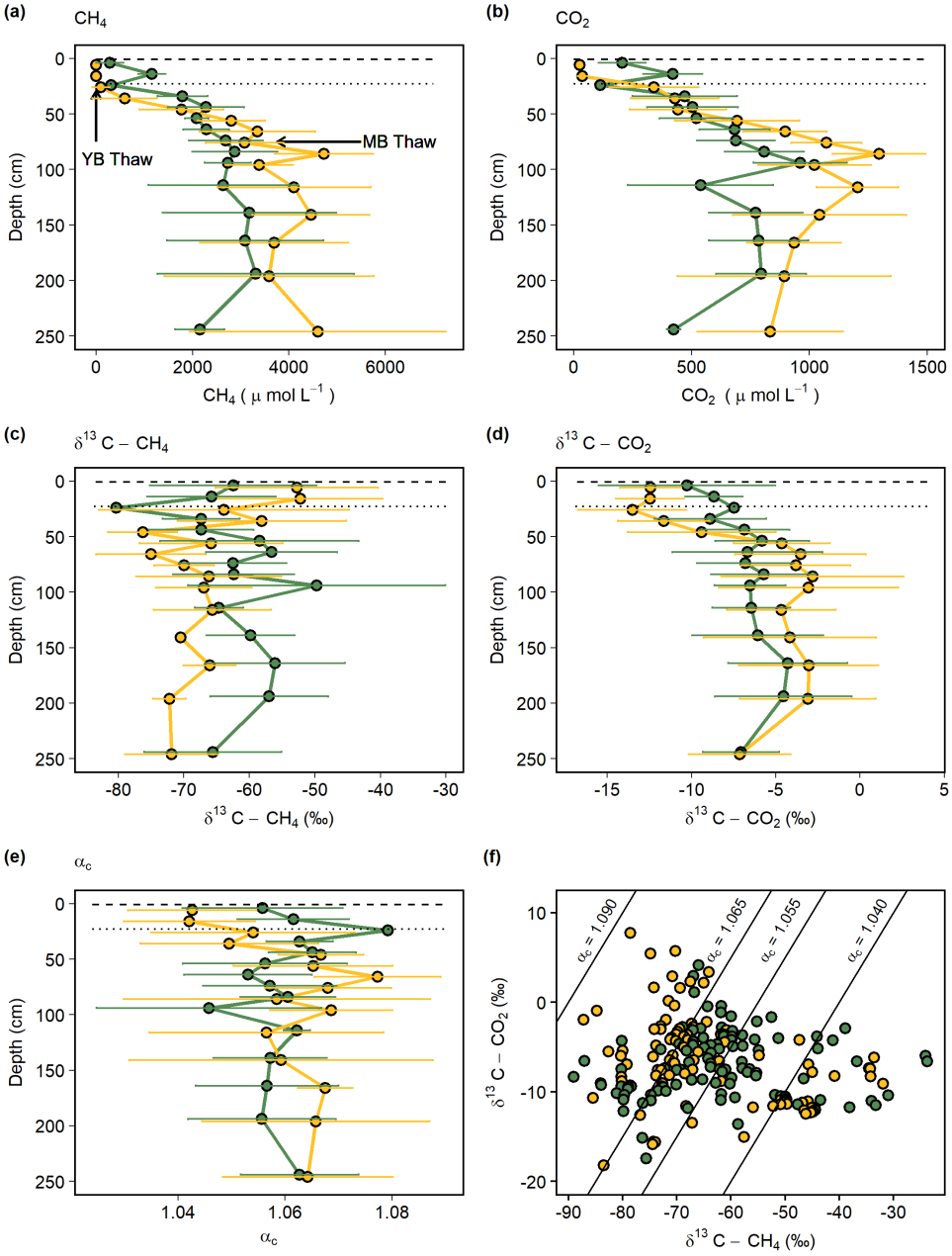

513

514 **Figure 2.** Average seasonal (May – September) depth profiles in the young (green, black
515 circles) and mature (yellow, black circles) bog of (a) dissolved CH_4 concentration (μmol L^{-1}),
516 (b) dissolved CO_2 concentration (μmol L^{-1}), (c) $\delta^{13}C$-CH_4 (‰), (d) $\delta^{13}C$-CO_2 (‰), and (e)

https://doi.org/10.5194/bg-2021-337
Preprint. Discussion started: 11 January 2022

517 apparent fractionation factor (α_c) between dissolved CH_4 and CO_2. (f) Cross-plot of
518 corresponding $\delta^{13}C$-CH_4 and $\delta^{13}C$-CO_2 values (‰) in the young bog and mature bog, from
519 raw data used in panels (c) and (d). Diagonal lines represent different α_c where α_c 1.040 –
520 1.065 represents acetoclastic methanogenesis, and α_c 1.055 – 1.09 represents
521 hydrogenotrophic methanogenesis (Whiticar, 1999). (a) – (e) Dashed and dotted horizontal
522 lines represent water table depth in the young (YB) and mature bog (MB) respectively.
523 Arrows in panel (a) represent depth of thaw transition in both the young (29 cm) and mature
524 bog (71 cm), i.e., the transition from deep peat (accumulated prior to thawing) and shallow
525 peat (accumulated post thawing).

526

527 The young bog and mature bog had distinct profiles of ^{13}C isotopic signatures for both
528 CH_4 and CO_2 (Figure 2c, d). The young bog had no apparent trend in ^{13}C-CH_4 by depth,
529 averaging -62.4 ± 7.0 ‰ and ranging between -49.7 ‰ and -80.3 ‰ (Figure 2c). In the
530 mature bog we observed isotopically heavy ^{13}C-CH_4 above the water table, which suggested
531 influence from CH_4 oxidation. Under the water table, the mature bog had significantly lighter
532 ^{13}C-CH_4 compared to the young bog at an average of -68.7 ± 5.0 ‰ and -62.4 ± 7.0 ‰,
533 respectively ($F_{(1, 92)} = 17.25$, $P < 0.001$). In the young bog, ^{13}C-CO_2 had no apparent trend
534 with depth (average -6.8 ± 1.6 ‰). The mature bog had isotopically lighter ^{13}C-CO_2 above
535 the water table and was isotopically heavier than the young bog below the water table ($F_{(1, 99)}$
536 $= 5.33$, $P < 0.05$).

537 The apparent fractionation factor (α_C) is a robust parameter to characterize the relative
538 contribution of CH_4 production pathways, with values of 1.040 – 1.060 indicating
539 acetoclastic methanogenesis and 1.060 – 1.090 for hydrogenotrophic methanogenesis
540 (Chanton et al., 2005). Similar to the gas ^{13}C depth-profiles, we found no clear trend in α_C
541 with depth in the young bog with an average of 1.058 ± 0.012 and range of 1.018 – 1.079
542 (Figure 2e). In the mature bog, the average α_C was lowest in samples collected above the
543 water table at 5, 15, and 25 cm, likely due to the influence of CH_4 oxidation. The average α_C
544 beneath the water table in the mature bog was 1.064 ± 0.017 and ranged from 1.015 – 1.094,
545 similar to the average values found in the young bog ($F_{(1, 99)} = 0.7$, $P = 0.4$).

https://doi.org/10.5194/bg-2021-337
Preprint. Discussion started: 11 January 2022

In the isotopic ratio cross-plot of $\delta^{13}C\text{-}CH_4$ and $\delta^{13}C\text{-}CO_2$ (Figure 2f), most of the young bog had α_C values of between 1.055 – 1.065 (29 in total), with a greater number of samples (21) between α_C =1.040 – 1.055, compared to the mature bog (15). In contrast, a greater proportion of the mature bog samples had α_C >1.065 (42 in the young bog and 52 in the mature bog). There was no clear depth trend in the α_C values and no samples in this study had α_C >1.090. Several samples (13) from the young bog and mature bog had α_C values of <1.040, likely due CH_4 oxidation (Knorr et al., 2009). Overall, the isotopic data indicates a general dominance of hydrogenotrophic methanogenesis in both sites, but a greater contribution of acetoclastic methanogenesis in the young bog relative to the mature bog.

3.3 Magnitude and isotopic signature of land-atmosphere gas fluxes

The young bog had almost three times greater average CH_4 fluxes than the mature bog during the May – September study period, at 82.3 ± 21.9 mg CH_4 m^{-2} and 30.8 ± 10.6 mg CH_4 m^{-2} day^{-1}, respectively (Figure 3a). Fluxes of CH_4 in the young bog were greatest between June and August, ranging from 80.6 ± 40.3 mg CH_4 m^{-2} day^{-1} to 100.9 ± 63.1 mg CH_4 m^{-2} day^{-1}. The lowest young bog CH_4 fluxes were observed in September at 55.0 ± 17.7 mg CH_4 m^{-2} day^{-1} (Figure S3a). Mature bog CH_4 fluxes were greatest in September (55.8 ± 21.1 mg CH_4 m^{-2} day-1) and lowest in May (5.6 ± 2.7mg CH_4 m^{-2} day^{-1}). Ecosystem respiration (CO_2 emissions measured with dark chambers) was significantly lower in the young bog than mature bog, with study period averages of 0.6 ± 0.3 and 1.9 ± 0.3 g CO_2 m^{-2} day^{-1}, respectively (Figure S2b). Maximum ecosystem respiration in the young bog occurred in August (1.6 g CO_2 m^{-2} day^{-1}) and was much lower during the other four months (monthly averages of 0.2 to 0.4 g CO_2 m^{-2} day^{-1}). Maximum ecosystem respiration in the mature bog was found for the period June to August (monthly averages between 2.1 and 2.6 g CO_2 m^{-2} day^{-1}), with lower emissions in September (0.8 g CO_2 m^{-2} day^{-1}). The proportion of total C

https://doi.org/10.5194/bg-2021-337
Preprint. Discussion started: 11 January 2022

570 emissions (sum of CH4 and CO2 emissions) released as CH_4 was an order or magnitude
571 greater in the young bog than mature bog stage, at 18 and 2% respectively, resulting from
572 both the young bog higher CH4 emissions and lower ecosystem respiration (Figure S3). The
573 δ^{13}C-CH_4 signature of CH_4 emissions (intercept values from Keeling plots), in the young bog
574 were significantly greater than those observed in the mature bog (Figure 3c; $F_{(1, 4)} = 20.67$, P
575 < 0.05)., suggesting a greater influence of acetoclastic CH_4 production. The average isotopic
576 signature in young bog CH_4 emissions (n = 4) was -66.5 ± 1.4‰ (Figure 3c), whereas the
577 average from mature bog emissions (n = 4) was -78.5 ± 5.6‰ (95% CI).

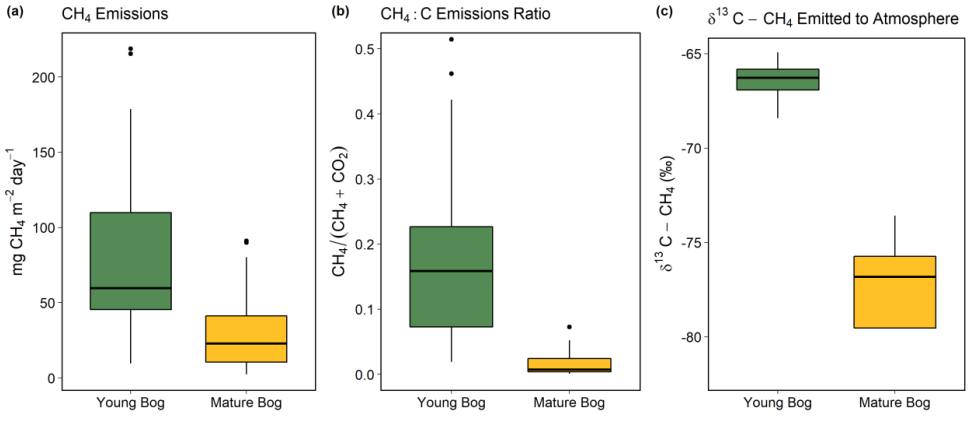

578

579 **Figure** 3. Magnitude and isotopic signature of greenhouse gas fluxes from the young bog
580 (green) and mature bog (yellow) shown as boxplots. Boxes represents the interquartile range
581 (25 – 75%), with median shown as black horizontal line. Whiskers extend to 1.5 times the
582 interquartile range (distance between first and third quartile) in each direction, with outlier
583 data plotted individually as black dots (a) The magnitude of net land-atmosphere CH_4
584 emissions as measured by soil chambers. (b) The ratio between CH_4 emissions and the sum of
585 CO_2 emissions (ecosystem respiration) and CH_4, both standardized to per g C. (c) Intercept
586 values of Keeling plots indicating the δ^{13}C-CH_4 signature of CH_4 emissions. Isotopically
587 heavier (i.e., less negative) δ^{13}C-CH_4 is produced via acetoclastic methanogenesis, whereas
588 isotopically lighter (i.e., more negative) δ^{13}C-CH_4 is produced via hydrogenotrophic
589 methanogenesis, The CH_4 and CO_2 land-atmosphere fluxes shown in (a) and (b) were
590 measured once a month from May – September 2018. The δ^{13}C-CH_4 of CH_4 emitted to the
591 atmosphere was measured in September and October 2016 (see methods for details and
592 Figure S4 for Keeling plots).

593

https://doi.org/10.5194/bg-2021-337
Preprint. Discussion started: 11 January 2022

3.4 Microbial community structure along the permafrost peatland thaw gradient

We used NMDS ordinations to assess differences in microbial community structure between solid peat and pore water samples, between sampling depths, and between the plateau, young bog, and mature bog. The only exception was the plateau, where only peat samples were collected (i.e,. no pore water samples). Microbial community structure in peat was determined to be significantly different from porewater microbial communities (PERMANOVA $P < 0.05$, Figure 4). The differences observed in the microbial community structure between peat and pore water samples could be a function of the different extraction methods used to extract DNA (Carrigg et al., 2007). Among the pore water samples, distinct microbial communities were found to be associated with the young bog and mature bog. Similarly, microbial community structure in peat was found to be significantly distinct between the three successional stages (plateau peat, young bog and mature bog; Figure 4; PERMANOVA, $P < 0.05$). There is also a common trend in vertical community structuring for all sample matrices according to depth. Changes in overall microbial community composition in both peat and pore water, across a vertical profile (to a maximum depth of 160 cm), illustrate a confluence in microbial community structure with depth in both the young and mature bog (Figure 4). In other words, community structure was most dissimilar at depths closer to the surface (Figure 4, Figure S2b, c; PERMANOVA; $P < 0.05$). This trend was particularly evident in the porewater samples (Figure 4). In the peat samples, though microbial communities did not fully converge, deeper young bog peat (i.e., 90 – 160 cm) communities did become more similar to communities found in the mature bog at intermediate depths (i.e., 30 – 70 cm), based on the nearness of sample points on the NMDS (Figure 4). We also observed that the mature bog near-surface peat samples were located closer to the plateau peat on the NMDS (Figure 4, ANOSIM; $P = 0.266$). It was not possible to assess the presence of this cyclic succession (from young bog to mature bog to plateau) in

https://doi.org/10.5194/bg-2021-337
Preprint. Discussion started: 11 January 2022

the pore water samples since we did not characterize the microbial community in the plateau pore water. Finally, we also assessed the effect of seasonality on microbial community diversity and found no effect with regards to sampling month (ANOSIM; $P = 0.559$).

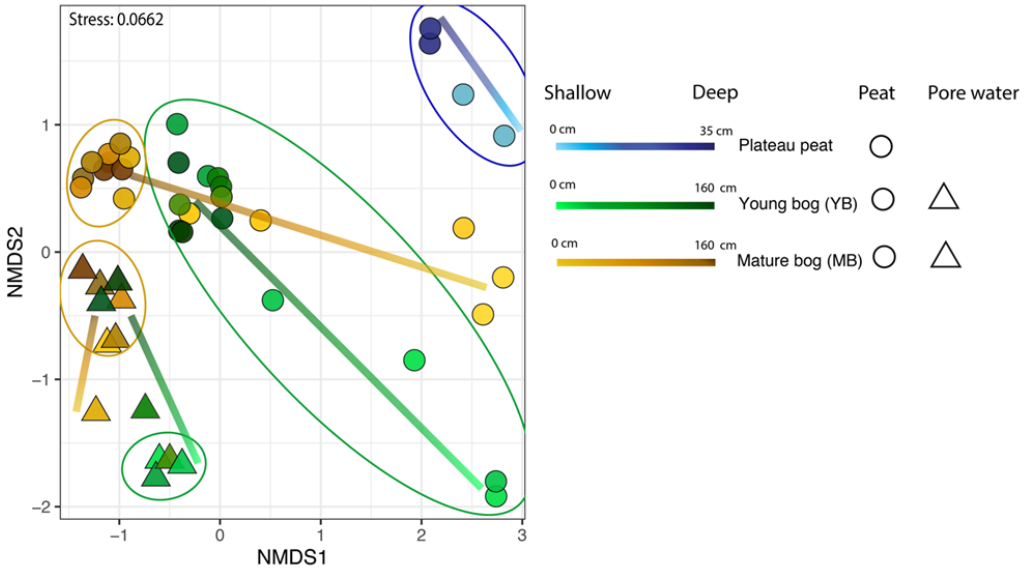

Figure 4. Microbial community distribution according to stage of peat/pore water. NMDS ordinations of amplicon sequencing variant (ASV) data demonstrate significant community dissimilarities (PERMANOVA; $P < 0.05$) according to thaw stage for both pore water (shown by the triangles) and peat (shown by the circles) samples, encircled by 95% confidence intervals. Colour gradient and lines demonstrate the shift in microbial community structure along vertical depth profiles where lighter shades indicate samples closer to the surface.

The total archaeal community comprised 6% of the entire microbial dataset. Methanogen-related orders comprised 54% of this archaeal dataset and demonstrated marked differences in the relative abundance of acetoclastic-related methanogens according to thaw stage and depth in both peat and pore water samples (Figure 5; Figure S2). In the young and mature bog peat samples, hydrogenotrophic-related methanogens were ubiquitously present throughout both depth profiles (Figure 5a). In comparison, acetoclastic-related methanogens exhibited a relatively restricted presence, only present at specific depths (Figure 5a). These

https://doi.org/10.5194/bg-2021-337
Preprint. Discussion started: 11 January 2022

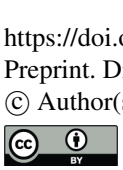

communities were most abundant (>25% of the total methanogenic community) near the surface in the young bog, just above and below the thaw transition zone (Figure 5a). In the pore water, hydrogenotrophic methanogens were also dominant throughout depths in both stages of thaw (Figure 5b). However, in contrast to peat samples, acetoclastic methanogens were virtually absent in the pore water, although minimally present (i.e., ≤ 10% relative abundance) at depths between 35 and 155 cm, all found below the thaw transition zone (Figure 5b).

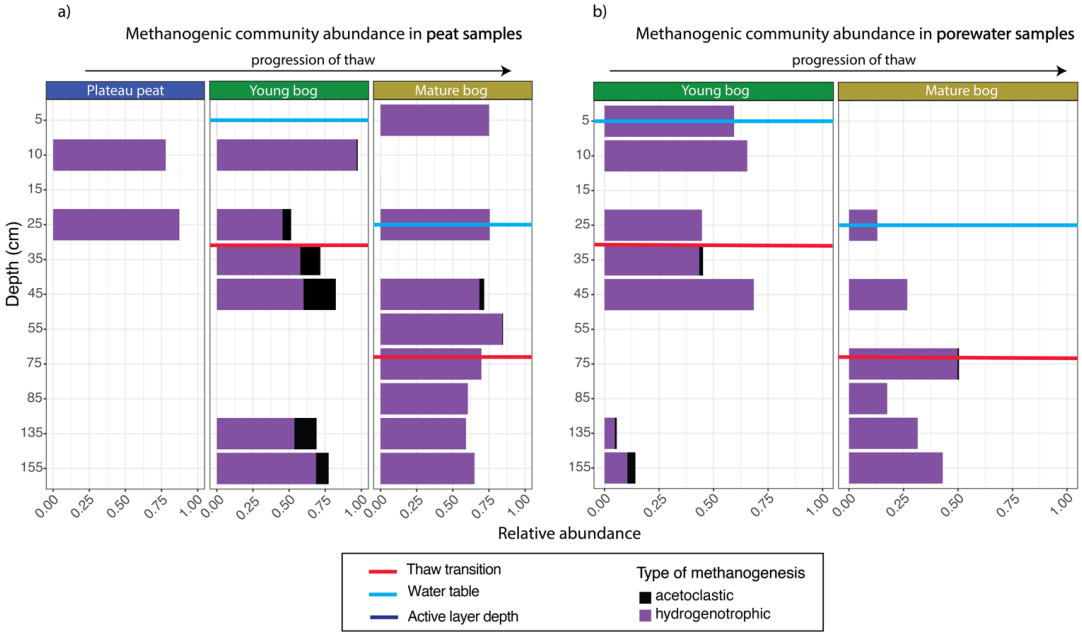

Figure 5. Relative abundance of archaeal orders according to putative methanogenic capability, along a depth profile for peat and pore water samples. Samples are arranged according to depth (y axis), with the relative abundance of methanogenic archaea resolved shown on the x axis. Note that the y axis does not uniformly progress in 10 cm increments. Progression of thaw is shown from plateau peat to young bog to mature bog at the top of the figures, with position of water table shown in blue for each panel. Red lines demonstrate thaw transition zone for the young bog and mature bog. (a) Stacked bar plot of methanogenic Archaea for all peat samples. Samples demonstrate significant differences in putative methanogen composition between all stages (Kruskall-Wallis test & Wilcox rank sum test, with Benjamini-Hochberg corrected p-values, $P < 0.05$). (b) Stacked bar plot of methanogenic Archaea for all pore water samples. Samples do not demonstrate significant

https://doi.org/10.5194/bg-2021-337
Preprint. Discussion started: 11 January 2022

differences in putative methanogen composition between stages (Kruskall-Wallis test, with Benjamini-Hochberg corrected p-values, $P = 0.965$).

Using a redundancy analysis (RDA, Figure 6) we found that 27.6% of variation in the methanogenic community was explained by two variables: thaw stage (ANOVA, $P < 0.05$) and depth from the water table (ANOVA, $P < 0.05$). This percentage is in accordance with other studies conducted in permafrost impacted regions using similar methods, where the percentage of explained variation falls between 6% (low) to 43% (high) (Comte et al., 2015; Hough et al., 2020). Next, we used variance partitioning to assess the extent to which thaw stage and depth from the water table (i.e. the significant environmental variables identified by the RDA) explained the variation in only the methanogenic community structure (Figure 6). Based on this analysis, thaw stage explained 18.4% and distance to the water table explained 4.3% of methanogenic community variation, respectively.

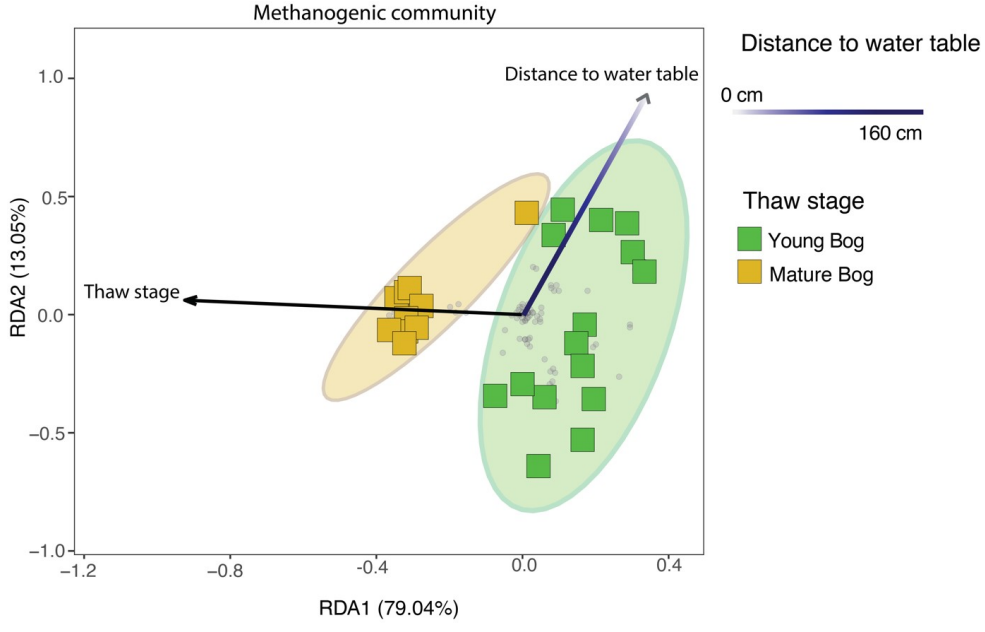

Figure 6. Redundancy analysis (RDA) exploring biotic and abiotic variables influencing the total methanogenic community (adjusted $R^2 = 27.6\%$) in the peat and pore water samples**.** Grey dots in the panel demonstrate the distribution of all ASVs in the methanogenic dataset. Shaded ellipses represent the 95% confidence intervals for microbial community diversity

https://doi.org/10.5194/bg-2021-337
Preprint. Discussion started: 11 January 2022

694 according to peatland thaw stage (young bog vs mature bog). Only significant (ANOVA, $P <$
695 0.05) variables are shown. Using variation partitioning, we found that peatland thaw stage
696 significantly explains about 18.4% of methanogenic community variation whereas distance to
697 water table explained 4.3%. Both axes are significant (ANOVA, $P < 0.05$).
698

699 ## 4. Discussion

700 Our study shows that high CH_4 emissions from thermokarst bogs in the initial decades
701 following permafrost thaw (young bog) are not only linked to environmental conditions
702 (wetness, soil temperature, vegetation), but also driven by relatively increased microbial CH_4
703 production through the energetically more favourable acetoclastic methanogenesis pathway.
704 Evidence of acetoclastic methanogens and CH_4 produced via the acetoclastic metabolic
705 pathway was found in the young bog both near the surface and at depths below the thaw
706 transition (i.e., in peat that accumulated prior to permafrost thaw). We are unable to
707 determine whether these greater CH_4 emissions in the initial decades following thaw are due
708 to the mineralization of labile organic matter released from previously frozen peat, or are
709 driven solely by fresh, labile DOM derived from surface vegetation leached throughout the
710 peat profile. Elevated CH_4 emissions then slow over the following centuries with succession
711 into a mature thermokarst bog stage where CH_4 production is almost exclusively through the
712 hydrogenotrophic pathway.

713 ### *4.1 Shift in microbial community assemblages along a permafrost thaw gradient*

714 Microbial communities varied along the permafrost thaw gradient; among different thaw
715 stages (permafrost peat plateau, young bog, and mature bog), with peat depth (surface down
716 to 160 cm), and between different sample types (solid peat and pore water). We found clear
717 differences in microbial communities between the young bog and mature bog, despite similar
718 peat stratigraphy up t the surficial vegetation (Heffernan et al., 2020), where dominant
719 *Sphagnum* species varied. The greater height of the peat surface above the water table and

https://doi.org/10.5194/bg-2021-337
Preprint. Discussion started: 11 January 2022

720 relatively drier conditions in the mature bog, due to the slow accumulation of new peat over
721 centuries, leads to a shift in vegetation composition from hydrophilic *Sphagnum* and
722 graminoids towards more drought resistant *Sphagnum* spp. and ericaceous shrubs. This shift
723 in water table position and vegetation community, along with a decrease in temperatures
724 (Figure S1a) due to the thermal insulating properties of *Sphagnum* peat (Kujala, Seppälä, &
725 Holappa, 2008) appears to have caused the observed differences in microbial communities
726 between the young and mature bog, even at depths >1 m. Microbial communities were most
727 dissimilar between the peat plateau and young bog. This was unsurprising given the abrupt
728 shift from the elevated, frozen, and relatively dry peat plateau forest to the young bog where
729 the surface was saturated, dominated by hydrophilic vegetation and had warmer
730 temperatures. We further noted that the microbial community of the mature bog was more
731 similar with the peat plateau than with the young bog. Paleo-records in the region (Heffernan
732 et al., 2020; Pelletier et al., 2017; Zoltai, 1993) show that many peatlands have undergone
733 cyclical permafrost developments, as thermal insulating properties of *Sphagnum* peat in
734 mature bogs leads to the re-aggradation of permafrost peat plateaus. Our study suggests that
735 the peat plateau microbial community is influenced by the preceding mature bog microbial
736 community as permafrost aggrades.

737 The most dissimilar microbial community composition was observed between
738 samples near the surface and those at depth (i.e., down to 160 cm), as has been also observed
739 in other permafrost ecosystems (Frey et al., 2016; Monteux et al., 2018). Shifts in microbial
740 community composition along the thaw gradient were most evident nearer the surface,
741 whereas communities found at depth were similar between the young bog and mature bog
742 (Figure 4). At the surface, microbial community structure is influenced by the successional
743 vegetation community (Hodgkins et al., 2014) and the role that vegetation has on microbial
744 community structure has been well documented in northern peatlands (Robroek et al., 2015,

https://doi.org/10.5194/bg-2021-337
Preprint. Discussion started: 11 January 2022

745 2021). In contrast, communities at depth are known to be influenced by peat properties, such
746 as peat chemistry and degree of decomposition, and the paleoenvironment under which they
747 originally colonized (Lee et al., 2012; Holm et al., 2020). In the young and mature bog both
748 peat properties (humification indices including FTIR 1630/1090 cm^{-3} and C:N ratios) and the
749 paleoenvironment at depth are similar (Heffernan et al., 2020), which may explain the
750 observed convergence of microbial community structure. Nonetheless, although there are
751 some similarities at depth between both young and mature bog, microbial communities
752 inhabiting either are still distinct (Figure 4). This is emphasized by the differing abundance of
753 Archaea that participate in hydrogenotrophic or acetoclastic methanogenesis (Figure 5) in
754 both stages down the peat profile.

755 As has been shown previously in other thermokarst peatlands (McCalley et al., 2014),
756 the young and mature bog stages were dominated by hydrogenotrophic methanogens.
757 However, acetoclastic methanogens were relatively more abundant in the young bog (Figure
758 5), particularly at or below the transition into peat that accumulated prior to permafrost thaw.
759 Thaw stage and distance from the water table were found to influence the methanogenic
760 community composition (Figure 6), with distance from the water table dictating where anoxic
761 conditions persist (Blodau et al., 2004) and thus where methanogenic colonization can occur.
762 The influence of vegetation communities associated with different thermokarst peatland
763 stages on methanogenic community composition has previously been attributed to the role of
764 plant derived DOM serving as the substrate for CH_4 production (Liebner et al., 2015;
765 McCalley et al., 2014). The presence of hydrophilic vegetation, particularly graminoids, in
766 the saturated young bog provides the precursors for fermentation, yielding acetate (Liebner et
767 al., 2015; Strom et al., 2015) and serving as the substrate for acetoclastic CH_4 production.
768 The downward transport from the surface of labile, plant derived DOM in the young bog

https://doi.org/10.5194/bg-2021-337
Preprint. Discussion started: 11 January 2022

769 (Chanton et al., 2008) likely provides sufficient acetate for the establishment of acetoclastic
770 methanogens at depth in this environment.

771 *4.2 Production and emissions of CH_4 along a peatland thaw gradient*

772 Isotopic signatures of dissolved CO_2 and CH_4 in porewater and of CH_4 emitted to the
773 atmosphere provided further evidence of relatively elevated acetoclastic methanogenesis in
774 the young bog stage. The general increase in $^{13}C\text{-}CO_2$ with depth observed at both sites
775 (Figure 2d) indicates accumulation of isotopically heavier $^{13}C\text{-}CO_2$ which is likely explained
776 by the preferential use of isotopically lighter $^{13}C\text{-}CO_2$ during hydrogenotrophic
777 methanogenesis (Hornibrook et al., 2000). As a result, CH_4 tends to become lighter with
778 depth and this was particularly apparent in the mature bog (Figure 2c). Together, the $^{13}C\text{-}CH_4$
779 and $^{13}C\text{-}CO_2$ data and the resulting α_C depth profiles suggest that the majority of CH_4 is
780 produced via the hydrogenotrophic methanogenic pathway, which supports the findings of
781 the microbial community analysis (Figure 5). Our isotope data also suggests that a greater
782 proportion of CH_4 is produced via acetoclastic methanogenesis throughout the profile in the
783 young bog compared to the mature bog, which again agrees with the relatively greater
784 abundance of acetoclastic methanogens observed at that site (Figure 5).

785 In this study we found that average CH_4 emissions in the initial decades following thaw,
786 in the young bog stage, were 2.5 – 3 times greater than emissions measured in the mature bog
787 stage which had thawed ~200 years ago (Figure 3a). Furthermore, the proportion of CH_4 to
788 overall C emissions (Figure 3b) was considerably greater in the young bog than in the mature
789 bog. In the mature bog the lower water table position leads to both increased CO_2 emissions
790 and decreasedCH_4 emissions, resulting in a reduced fraction of C emissions as CH_4. Previous
791 studies have shown similarly increased CH_4 emissions in the initial decades following thaw
792 (Johnston et al., 2014; Wickland et al., 2006). Our study shows that these higher CH_4

https://doi.org/10.5194/bg-2021-337
Preprint. Discussion started: 11 January 2022

emissions are likely linked to increased wetness, temperatures, and more labile organic matter which favour a greater proportion of CH_4 produced via acetoclastic methanogenesis, as shown by our $\delta^{13}C$-CH_4, α_c depth profiles and microbial community composition analyses.

Many factors, including environmental conditions and microbial community structure likely contribute to the differences in net CH_4 emissions from the young and mature bog (Figure 3a). Methane oxidation has been shown to be an important regulator of post-thaw CH_4 emissions (Perryman et al., 2020) and to result in isotopically heavier (i.e., less negative) $\delta^{13}C$-CH_4 and lighter (i.e., more negative) $\delta^{13}C$-CO_2 (Whiticar, 1999). Our data suggests the role of CH_4 oxidation was different between sites. Methane oxidation was apparent in the $\delta^{13}C$-CH_4 and $\delta^{13}C$-CO_2 signatures above the water table in the mature bog but no CH_4 oxidation is evident in the young bog (Figure 2c, d). The difference in gas flux $\delta^{13}C$ signatures (Figure 3c) also suggests a greater prevalence of CH_4 oxidation in the mature bog. However, the observed differences between the young and mature bog CH_4 emissions and depth profiles are likely not due solely to increased CH_4 oxidation above the water table in the mature bog. The lower CH_4 emissions and greater dominance of hydrogenotrophic methanogenesis in the mature bog relative to the young bog presumably arise from lower soil temperatures, a vegetation shift and associated reduction in labile C substrates as peat aggrades in the mature bog in addition to a deeper water table that contributes both to lower CH_4 production and higher potential for CH_4 oxidation. However, using this interdisciplinary approach, we are unable to determine the relative contribution of acetoclastic methanogenesis at each depth to the overall emissions at the surface.

Our results, and those of others (Euskirchen et al., 2014; Johnston et al., 2014), have shown that CH_4 emissions exhibit seasonal variation (Figure S2b). However, in contrast to some previous findings (Ebrahimi & Or, 2017), we did not observe a corresponding seasonal response in the microbial community composition (Figure S3a). This may be a sampling

https://doi.org/10.5194/bg-2021-337
Preprint. Discussion started: 11 January 2022

design effect since our study spanned only two months (June and September). However, other studies have also shown that soil microbial community growth is not impacted by seasonal variations in temperature (Simon et al., 2020) and that microbial communities require a longer time scale (years-decades-centuries) to respond to temperature following thaw (Feng et al., 2020). Our results corroborate these observations, suggesting a long-term response in the microbial community composition to the ecological shifts associated with autogenic peatland succession following permafrost thaw. Autogenic peatland succession following thaw occurs on the decade to century timescale, shifting from recently thawed to mature thermokarst bogs (Camill, 1999). Both recently thawed (young) and mature thermokarst bogs have distinct hydrological regimes, vegetation communities, and peat chemistry. Following thaw, associated changes in vegetation and litter input alters microbial community composition and activity (Adamczyk, Perez-Mon, Gunz, & Frey, 2020; Kirkwood et al., 2021). Such changes in microbial community structure thus impact CH_4 emissions from thermokarst peatlands. Under predicted climatic warming scenarios differences in microbial community composition have been shown to be increasingly driven by seasonally independent variables such as substrate quality and the legacy effects of soil temperatures (Luláková et al., 2019). This study suggests that the ecological conditions required for increased methanogenic activity at depth is limited to the initial decades following thaw, after which the microbial community structure changes in response to lowering of the water table, lower soil temperatures and shifts in the vegetation community.

5. Conclusion

This study demonstrates that higher CH_4 emissions in thermokarst bogs in the initial decades following thaw are driven by shifts in vegetation communities that produce organic matter inputs of varying lability (Burd et al., 2020) and prevalence of anoxic conditions,

https://doi.org/10.5194/bg-2021-337
Preprint. Discussion started: 11 January 2022

842 which was associated with an increase of acetoclastic methanogenesis in our site. The
843 influence of this pathway was apparent at depth throughout the peat profile. With succession
844 following thaw towards a mature thermokarst bog, a shift in water table position and
845 vegetation composition seems to reduce the role of acetoclastic methanogenesis pathway.
846 Average growing season CH_4 emissions were 2.5 – 3 times greater in the recently thawed
847 young bog. Overall, C emissions in the young bog contained proportionally more CH_4 than
848 those from the mature bog, due to greater CH_4 production and also reduced CO_2 emissions.
849 These greater CH_4 emissions in the young bog are driven by a higher contribution to surface
850 emissions from CH_4 produced throughout the peat profile by acetoclastic methanogens. The
851 response of the microbial community to permafrost thaw is tied to the shifting ecological
852 conditions associated with peatland autogenic succession. Warmer and wetter conditions in
853 the initial decades following thaw, in conjunction with a greater availability of labile plant
854 leachates, provides favourable conditions for acetoclastic methanogens throughout the peat
855 profile. Given the projected increases in thermokarst peatland formation (Olefeldt et al.,
856 2016), our study suggests that we can expect a pulse of CH_4 emissions from current regions
857 of the discontinuous permafrost zone. This pulse will be driven, in part, by increased
858 acetoclastic methanogenesis from labile substrates in recently thawed thermokarst peatlands.
859 However, this rapid increase in CH_4 emissions will only remain at the decadal to century
860 scale as autogenic peatland succession results in relatively drier mature thermokarst bogs,
861 where lower temperatures and less labile substrate availability leads to a dominance of
862 hydrogenotrophic methanogenesis.
863

864 **Data availability**

865 All biogeochemical and enzyme datasets generated and analyzed during this study are
866 available in the UAL Dataverse repository, [https://doi.org/10.5683/SP3/5TSH9V]. Microbial

https://doi.org/10.5194/bg-2021-337
Preprint. Discussion started: 11 January 2022

867 sequences used in this study can be accessed from the NCBI database, using accession
868 number PRJNA660023.
869

870 **Author contributions**

871 All authors contributed to the conception of the work. LH and CEA performed the field work
872 component. LH performed the biogeochemistry measurements. MAC performed the
873 microbial measurements. LH and MAC analyzed the data and wrote the manuscript draft. All
874 authors reviewed and edited the manuscript.

875 **Competing interests**

876 The authors declare that they have no conflict of interest.

877 **Acknowledgements**

878 The authors wish to that McKenzie Kuhn, Maya Frederickson, Jördis Stührenberg, and Trisha
879 Elliot for assistance with field and lab work. We also thank Sophie Dang, at MBSU for
880 providing guidance throughout 16S rRNA gene library building and for subsequently
881 sequencing these libraries at the MBSU facility.

882 **Financial support**

883 Funding and support were provided to D. Olefeldt and M. Bhatia by the Natural Science and
884 Engineering Research Council of Canada, Discovery grant (RGPIN-2016-04688 to DO and
885 RGPIN-2020-05975 to MB) and the Campus Alberta Innovates Program (CAIP).

886
887
888

https://doi.org/10.5194/bg-2021-337
Preprint. Discussion started: 11 January 2022

References

Adamczyk, M., Perez-Mon, C., Gunz, S., & Frey, B. (2020). Strong shifts in microbial community structure are associated with increased litter input rather than temperature in High Arctic soils. Soil Biology and Biochemistry, 151. https://doi.org/10.1016/j.soilbio.2020.108054

Allan, E., Manning, P., Alt, F., Binkenstein, J., Blaser, S., Blüthgen, N., … Fischer, M. (2015). Land use intensification alters ecosystem multifunctionality via loss of biodiversity and changes to functional composition. Ecology Letters. https://doi.org/10.1111/ele.12469

Beilman, D. W. (2001). Plant community and diversity change due to localized permafrost dynamics in bogs of western Canada. Canadian Journal of Botany, 79(8), 983–993. https://doi.org/10.1139/cjb-79-8-983

Bellisario, L. M., Bubier, J. L., Moore, T. R., & Chanton, J. P. (1999). Controls on CH4 emissions from a northern peatland. Global Biogeochemical Cycles, 13(1). https://doi.org/10.1029/1998GB900021

Berghuis, B.A., Yu, F.B., Schulz, F., Blainey, P.C.,, Woyke, T., Quake, S.R. (2019). Hydrogenotrophic methanogenesis in archaeal phylum Verstraetearchaeota reveals the shared ancestry of all methanogens. PNAS 116 (11): 5037-5044. https://doi.org/10.1073/pnas.1815631116

Blodau, C., Basiliko, N., & Moore, T. R. (2004). Carbon turnover in peatland mesocosms exposed to different water table levels. Biogeochemistry. https://doi.org/10.1023/B:BIOG.0000015788.30164.e2

Bridgham, S. D., Cadillo-Quiroz, H., Keller, J. K., & Zhuang, Q. (2013). Methane emissions from wetlands: Biogeochemical, microbial, and modeling perspectives from local to global scales. Global Change Biology. https://doi.org/10.1111/gcb.12131

Brown, J., Ferrians Jr., O. J., Heginbottom, J. A., & Melnikov, E. S. (1997). Circum-Arctic map of permafrost and ground ice conditions. USGS Numbered Series, 1. https://doi.org/10.1016/j.jallcom.2010.03.054

Burd, K., Estop-Aragonés, C., Tank, S. E., & Olefeldt, D. (2020). Lability of dissolved organic carbon from boreal peatlands: interactions between permafrost thaw, wildfire, and season. Canadian Journal of Soil Science, 13(February), 1–13. https://doi.org/10.1139/cjss-2019-0154

https://doi.org/10.5194/bg-2021-337
Preprint. Discussion started: 11 January 2022

929 Burger, M., Berger, S., Spangenberg, I., Blodau, C. (2016). Summer fluxes of methane and
930 carbon dioxide from a pond and floating mat in a continental Canadian peatland.
931 Biogeosciences. 13: 3777-3791. https://doi.org/10.5194/bg-13-3777-2016.
932
933 Cai, L., Alexeev, V.A., Arp, C.D., Jones, B.M., Liljedahl, A., Gadeke, A. (2016). Dynamical
934 Downscaling data for studying climactic impacts on hydrology, permafrost and ecosystem sin
935 Arctic Alaska. Earth System Science Data Discussion, doi:10.5194/tc-2016-87
936
937 Camill, P. (1999). Peat accumulation and succession following permafrost thaw in the Boreal
938 peatlands of Manitoba, Canada. Ecoscience, 6(4), 592–602.
939 https://doi.org/10.1080/11956860.1999.11682561
940
941 Carrigg, C., Rice, O., Kavanagh, S., Collins, G., O'Flaherty, V. (2007). DNA extraction
942 method affects microbial community profiles from soils and sediment. Applied Microbiology
943 and Biotechnology 77(4), 955-964.
944 Carroll, P., & Crill, P. (1997). Carbon balance of a temperate poor fen. Global
945 Biogeochemical Cycles. https://doi.org/10.1029/97GB01365
946
947 Chanton, J., Chaser, L., Glasser, P., & Siegel, D. (2005). Carbon and Hydrogen Isotopic
948 Effects in Microbial, Methane from Terrestrial Environments. Stable Isotopes and
949 Biosphere - Atmosphere Interactions, 85–105. https://doi.org/10.1016/B978-012088447-
950 6/50006-4
951
952 Chanton, J. P., Glaser, P. H., Chasar, L. S., Burdige, D. J., Hines, M. E., Siegel, D. I., …
953 Cooper, W. T. (2008). Radiocarbon evidence for the importance of surface vegetation on
954 fermentation and methanogenesis in contrasting types of boreal peatlands. Global
955 Biogeochemical Cycles, 22(4), 1–11. https://doi.org/10.1029/2008GB003274
956 Climate-Data.org. (2019). ة. Retrieved January 21, 2019, from 2019 website:
957 https://en.climate-data.org/north-america/canada/alberta/meander-river-11380/
958
959 Comte, J., Monier, A., Crevecoeur, S., Lovejoy,C., Vincent, W.F.(2015). Microbial
960 biogeography of permafrost thaw ponds across the changing northern landscape. Ecography
961 39, 609-618.
962
963 Connon, R.F., Quinton, W.L., Craig, J.R., Hayashi, M. (2014). Changing hydrologic
964 connectivity due to permafrost thaw in the lower Liard River valley, NWT, Canada.
965 Hydrological Processes 28(14): 4163-4178. https://doi.org/10.1002/hyp.10206
966
967 Conrad, R. (1999). Contribution of hydrogen to methane production and control of hydrogen
968 concentrations in methanogenic soils and sediments. FEMS Microbiology Ecology.
969 https://doi.org/10.1016/S0168-6496(98)00086-5
970
971 Corbett, J. E., Tfaily, M. M., Burdige, D. J., Cooper, W. T., Glaser, P. H., & Chanton, J.
972 P. (2013). Partitioning pathways of CO2 production in peatlands with stable carbon

973 isotopes. Biogeochemistry, 114(1–3). https://doi.org/10.1007/s10533-012-9813-1
974
975 Criquet, S., Farnet, A. M., Tagger, S., & Le Petit, J. (2000). Annual variations of
976 phenoloxidase activities in an evergreen oak litter: Influence of certain biotic and abiotic
977 factors. Soil Biology and Biochemistry. https://doi.org/10.1016/S0038-0717(00)00027-4
978
979 Dunn, C., Jones, T.G, Girard, A., Freeman, C. (2014). Methodologies for Extracellular
980 enzyme assays from wetland soils. Wetlands 34: 9-17 . https://doi.org/10.1007/s13157-013-
981 0475-0.
982
983 Ebrahimi, A., & Or, D. (2017). Mechanistic modeling of microbial interactions at pore to
984 profile scale resolve methane emission dynamics from permafrost soil. Journal of
985 Geophysical Research: Biogeosciences, 122(5). https://doi.org/10.1002/2016JG003674
986
987 Euskirchen, E. S., Edgar, C. W., Turetsky, M. R., Waldrop, M. P., & Harden, J. W.
988 (2014). Differential response of carbon fluxes to climate in three peatland ecosystems that
989 vary in the presence and stability of permafrost. Journal of Geophysical Research G:
990 Biogeosciences. https://doi.org/10.1002/2014JG002683
991
992 Feng, J., Wang, C., Lei, J., Yang, Y., Yan, Q., Zhou, X….Zhou, J. (2020). Warming-induced
993 permafrost thaw exarcerbates tundra soil carbon decomposition mediated by microbial
994 community. Microbiome 8(3), https://doi.org/10.1186/s40168-019-0778-3
995
996 Fisher, R. E., France, J. L., Lowry, D., Lanoisellé, M., Brownlow, R., Pyle, J. A., … Nisbet,
997 E. G. (2017). Measurement of the 13C isotopic signature of methane emissions from northern
998 European wetlands. Global Biogeochemical Cycles, 31(3).
999 https://doi.org/10.1002/2016GB005504
1000
1001 Fox, J., & Weisberg, S. (2011). An R Companion to Applied Regression, second ed.
1002 https://doi.org/10.1016/j.stomax.2010.07.001
1003
1004 Frey, B., Rime, T., Phillips, M., Stierli, B., Hajdas, I., Widmer, F., Hartmann, M. (2016).
1005 Micorbial diversity in European alpine permafrost nad active layers. FEMS microbiology
1006 Ecology. 92: doi.org/10.1093/femsec/fiw018
1007
1008 Fritze, H., Penttilä, T., Mäkiranta, P., Laiho, R., Tuomivirta, T., Forsman, J., … Peltoniemi,
1009 K. (2021). Exploring the mechanisms by which reindeer droppings induce fen peat methane
1010 production. Soil Biology and Biochemistry, 160.
1011 https://doi.org/10.1016/j.soilbio.2021.108318
1012
1013 Gibson, C. M., Chasmer, L. E., Thompson, D. K., Quinton, W. L., Flannigan, M. D., & amp.
1014 Olefeldt, D. (2018). Wildfire as a major driver of recent permafrost thaw in boreal
1015 peatlands. Nature Communications, 9(1). https://doi.org/10.1038/s41467-018-05457-1
1016

1017 Grant, R. F. (2015). Ecosystem CO2 and CH4 exchange in a mixed tundra and a fen within a
1018 hydrologically diverse Arctic landscape: 2. Modeled impacts of climate change. Journal of
1019 Geophysical Research: Biogeosciences, 120(7). https://doi.org/10.1002/2014JG002889
1020
1021 Hansen, A. M., Kraus, T. E. C., Pellerin, B. A., Fleck, J. A., Downing, B. D., & Bergamaschi,
1022 B. A. (2016). Optical properties of dissolved organic matter (DOM): Effects of biological and
1023 photolytic degradation. Limnology and Oceanography. https://doi.org/10.1002/lno.10270
1024
1025 Heffernan, L., Estop-Aragonés, C., Knorr, K.-H., Talbot, J., & Olefeldt, D. (2020).
1026 Long-term impacts of permafrost thaw on carbon storage in peatlands: deep losses offset by
1027 surficial accumulation. Journal of Geophysical Research: Biogeosciences, 2011(2865),
1028 e2019JG005501. https://doi.org/10.1029/2019JG005501
1029
1030 Heffernan, L., Jassey, V.E.J., Frederickson, M., Mackenzie, M.D., Olefeldt, D. (2021).
1031 Constraints on potential enzyme activitiws in thermokarst bogs: Implications for the carbon
1032 balance of peatlands following thaw. Global Change Biology, 27(19): 4711-4726.
1033 https://doi.org/10.1111/gcb.15758
1034
1035 Heginbottom, J. A., Dubreuil, M. H., & Harker, P. T. (1995). Canada, Permafrost. National
1036 Atlas of Canada.
1037
1038 Helbig, M., Pappas, C., & Sonnentag, O. (2016). Permafrost thaw and wildfire: Equally
1039 important drivers of boreal tree cover changes in the Taiga Plains, Canada. Geophysical
1040 Research Letters. https://doi.org/10.1002/2015GL067193
1041
1042 Helms, J.R., Stubbins, A., Ritchie, J.D., Minor, E.C., Kieber, D.J., Mopper, K. (2008).
1043 Absorption spectral slopes and slope rations as indicators of molecular weight, source, and
1044 photobleaching of chromophoric dissolved organic matter. Limnology and Oceanography,
1045 53(3): 955-969. https://doi.org/10.4319/lo.2008.53.3.0955
1046
1047 Hodgkins, S. B., Tfaily, M. M., McCalley, C. K., Logan, T. A., Crill, P. M., Saleska, S. R., …
1048 Chanton, J. P. (2014). Changes in peat chemistry associated with permafrost thaw
1049 increase greenhouse gas production. Proceedings of the National Academy of Sciences,
1050 111(16), 5819–5824. https://doi.org/10.1073/pnas.1314641111
1051
1052 Hoffman, G.E., Schadt, E.E. (2016). variancePartition: interpreting drivers of variance in
1053 complex gene expression studies. BMC bioinformatics 17(483).
1054 https://doi.org.10.1186/s12859-016-1323-z.
1055
1056 Holm, S., Walz, J., Horn, F., Yang, S., Grigoriev, M. N., Wagner, D., … Liebner, S. (2020).
1057 Methanogenic response to long-term permafrost thaw is determined by
1058 paleoenvironment. FEMS Microbiology Ecology, 96(3).
1059 https://doi.org/10.1093/femsec/fiaa021
1060

1061 Hopple, A. M., Wilson, R. M., Kolton, M., Zalman, C. A., Chanton, J. P., Kostka, J., …
1062 Bridgham, S. D. (2020). Massive peatland carbon banks vulnerable to rising
1063 temperatures. Nature Communications, 11(1). https://doi.org/10.1038/s41467-020-
1064 16311-8
1065
1066 Hornibrook, E. R. C., Longstaffe, F. J., & Fyfe, W. S. (1997). Spatial distribution of
1067 microbial methane production pathways in temperate zone wetland soils: Stable carbon
1068 and hydrogen isotope evidence. Geochimica et Cosmochimica Acta, 61(4), 745–753.
1069 https://doi.org/https://doi.org/10.1016/S0016-7037(96)00368-7
1070
1071 Hornibrook, E. R. C., Longstaffe, F. J., & Fyfe, W. S. (2000). Evolution of stable carbon
1072 isotope compositions for methane and carbon dioxide in freshwater wetlands and other
1073 anaerobic environments. Geochimica et Cosmochimica Acta, 64(6).
1074 https://doi.org/10.1016/S0016-7037(99)00321-X
1075
1076 Hough, M., McClure, A., Bolduc, B., Dorrepaal, E., Saleska, S., Klepac-Ceraj, V., Rich, V.
1077 (2020). Biotic and environmental drivers of plant microbiomes across a permafrost thaw
1078 gradient. Frontiers in Microbiology: https://doi.org/10.3389/fmicb.2020.00796
1079
1080 Huang, Y., Ciais, P., Luo, Y., Zhu, D., Wang, Y., Qiu, C., … Qu, L. (2021). Tradeoff of CO2
1081 and CH4 emissions from global peatlands under water-table drawdown. Nature Climate
1082 Change, 11(7). https://doi.org/10.1038/s41558-021-01059-w
1083
1084 Hugelius, G., Strauss, J., Zubrzycki, S., Harden, J. W., Schuur, E. A. G., Ping, C. L., …
1085 Kuhry, P. (2014). Estimated stocks of circumpolar permafrost carbon with quantified
1086 uncertainty ranges and identified data gaps. Biogeosciences, 11(23), 6573–6593.
1087 https://doi.org/10.5194/bg-11-6573-2014
1088 Jassey, V. E. J., Chiapusio, G., Gilbert, D., Toussaint, M. L., & Binet, P. (2012).
1089 Phenoloxidase and peroxidase activities in Sphagnum-dominated peatland in a warming
1090 climate. Soil Biology and Biochemistry, 46, 49–52.
1091 https://doi.org/10.1016/j.soilbio.2011.11.011
1092
1093 Johnston, C. E., Ewing, S. A., Harden, J. W., Varner, R. K., Wickland, K. P., Koch, J. C., …
1094 Jorgenson, M. T. (2014). Effect of permafrost thaw on CO2 and CH4 exchange in a
1095 western Alaska peatland chronosequence. ENVIRONMENTAL RESEARCH LETTERS,
1096 9(8). https://doi.org/10.1088/1748-9326/9/8/085004
1097
1098 Jones, M. C., Harden, J., O'Donnell, J., Manies, K., Jorgenson, T., Treat, C., & Ewing,
1099 S. (2018). Rapid carbon loss and slow recovery following permafrost thaw in boreal
1100 peatlands. Global Change Biology, 23(3), 1109–1127. https://doi.org/10.1111/gcb.13403
1101
1102 Juottonen, H., Kieman, M., Fritze, H., Hamberg, L., Laine, A. M., Merilä, P., … Tuittila, E.
1103 S. (2021). Integrating Decomposers, Methane-Cycling Microbes and Ecosystem Carbon

Fluxes Along a Peatland Successional Gradient in a Land Uplift Region. Ecosystems. https://doi.org/10.1007/s10021-021-00713-w

Kammann, C., Grünhage, L., & Jäger, H. J. (2001). A new sampling technique to monitor concentrations of CH4, N2O and CO2 in air at well-defined depths in soils with varied water potential. European Journal of Soil Science, 52(2). https://doi.org/10.1046/j.1365-2389.2001.00380.x

Kassambara, A., & Mundt, F. (2017). Package "factoextra." R Topics Documented.

Kassambara, A. (2018). ggpubr: "ggplot2" Based Publication Ready Plots. R package version 0.2. https://CRAN.R-project.org/package=ggpubr. Https://CRAN.R-Project.Org/Package=ggpubr. https://doi.org/R package version 0.1.8

Keeling, C. D. (1958). The concentration and isotopic abundances of atmospheric carbon dioxide in rural areas. Geochimica et Cosmochimica Acta, 13(4). https://doi.org/10.1016/0016-7037(58)90033-4

Keuper, F., van Bodegom, P.M., Dorrepaal, E., Weedon, J.T., van Hal, J., van Logtestijn, R. S.P., Aerts, R. (2012). A frozen feast : thawing permafrost increases plant-available nitrogen in subarctic peatlands. Global Change Biology, 18(6) :1998-2007. https://doi.org/10.1111/j.1365-2486.2012.02663.x

Keuper, F., Dorrepaal, E., van Bodegom, P.M., van Logtesijn, R., Venhuizen, G., van Hal, J., Aerts, R. (2017). Experimentally increased nutrient availability at the permafrost thaw front selectively enhances biomass production of deep-rooting subarctic peatland species. Global Change Biology 23(10) : 4257-4266. doi: 10.1111/gcb.13804

Kirkwood, J. A. H., Roy-Léveillée, P., Mykytczuk, N., Packalen, M., McLaughlin, J., Laframboise, A., & Basiliko, N. (2021). Soil Microbial Community Response to Permafrost Degradation in Palsa Fields of the Hudson Bay Lowlands: Implications for Greenhouse Gas Production in a Warming Climate. Global Biogeochemical Cycles, 35(6). https://doi.org/10.1029/2021GB006954

Knoblauch, C., Beer, C., Liebner, S., Grigoriev, M.N., Pfeiffer, E.M. (2018). Methane production as key to the greenhouse gas budget of thawing permafrost. Nature Climate Change, 8, 309-312. https://doi.org/10.1038/s41558-018-0095-z

Knorr, K. H., Lischeid, G., & Blodau, C. (2009). Dynamics of redox processes in a minerotrophic fen exposed to a water table manipulation. Geoderma, 153(3–4). https://doi.org/10.1016/j.geoderma.2009.08.023

Kotsyurbenko, O. R., Friedrich, M. W., Simankova, M. V., Nozhevnikova, A. N., Golyshin, P. N., Timmis, K. N., & Conrad, R. (2007). Shift from acetoclastic to H2-dependent

1148 methanogenesis in a West Siberian peat bog at low pH values and isolation of an
1149 acidophilic Methanobacterium strain. Applied and Environmental Microbiology, 73(7),
1150 2344–2348. https://doi.org/10.1128/AEM.02413-06
1151
1152 Kuhn, M., Varner, R., Bastviken, D., Crill, P., MacIntyre, S., Turetsky, M., … Olefeldt, D.
1153 (2021). BAWLD-CH₄: A Comprehensive Dataset of Methane
1154 Fluxes from Boreal and Arctic Ecosystems. Earth System Science Data Discussions.
1155 https://doi.org/10.5194/essd-2021-141
1156
1157 Kujala, K., Seppälä, M., & Holappa, T. (2008). Physical properties of peat and palsa
1158 formation. Cold Regions Science and Technology, 52(3).
1159 https://doi.org/10.1016/j.coldregions.2007.08.002
1160
1161 Lee, H., Schuur, E. A. G., Inglett, K. S., Lavoie, M., & Chanton, J. P. (2012). The rate of
1162 permafrost carbon release under aerobic and anaerobic conditions and its potential
1163 effects on climate. Global Change Biology, 18(2). https://doi.org/10.1111/j.1365-
1164 2486.2011.02519.x
1165
1166 Leroy, F., Gogo, S., Guimbaud, C., Bernard-Jannin, L., Hu, Z., & Laggoun-Défarge, F.
1167 (2017). Vegetation composition controls temperature sensitivity of CO2 and CH4 emissions
1168 and DOC concentration in peatlands. Soil Biology and Biochemistry, 107.
1169 https://doi.org/10.1016/j.soilbio.2017.01.005
1170
1171 Liebner, S., Ganzert, L., Kiss, A., Yang, S., Wagner, D., & Svenning, M. M. (2015).
1172 Shifts in methanogenic community composition and methane fluxes along the degradation of
1173 discontinuous permafrost. Frontiers in Microbiology, 6(MAY).
1174 https://doi.org/10.3389/fmicb.2015.00356
1175
1176 Luláková, P., Perez-Mon, C., Šantrůčková, H., Ruethi, J., & Frey, B. (2019). High-
1177 alpine permafrost and active-layer soil microbiomes differ in their response to elevated
1178 temperatures. Frontiers in Microbiology, 10(APR). https://doi.org/10.3389/fmicb.2019.00668
1179
1180 Masella, A. P., Bartram, A. K., Truszkowski, J. M., Brown, D. G., & Neufeld, J. D.
1181 (2012). PANDAseq : PAired-eND Assembler for Illumina sequences. (Figure 1), 1–7.
1182
1183 McCalley, C. K., Woodcroft, B. J., Hodgkins, S. B., Wehr, R. A., Kim, E. H., Mondav, R., …
1184 Saleska, S. R. (2014). Methane dynamics regulated by microbial community response to
1185 permafrost thaw. Nature, 514(7253), 478–481. https://doi.org/10.1038/nature13798
1186 McDonald, D., Price, M.N., Goodrich, J., Nawrocki, E.P., DeSantis,, T.Z., Probst, A.,
1187 Andersen, G.L., Knight, R., Hugenholtz, P. (2012). An improved Greengenes taxonomy with
1188 exzplicit ranks for ecological and evolutionary analyses of bacteria and archaea. ISME
1189 Journal 6: 610-618. https://doi.org/10.1038/ismej.2011.139
1190
1191 Monteux, S., Weedon, J. T., Blume-Werry, G., Gavazov, K., Jassey, V. E. J., Johansson, M.,

… Dorrepaal, E. (2018). Long-term in situ permafrost thaw effects on bacterial communities and potential aerobic respiration. ISME Journal. https://doi.org/10.1038/s41396-018-0176-z

Mudryk, L., Brown, R., Derksen, C., Luojus, K., Decharme, B., & Helfrich, S. (2018). Surface Air Temperature [in Arctic Report Card 2018]. Retrieved from https://www.arctic.noaa.gov/Report-Card

Nielsen, C.S,. Hasselquist, N.J, Nilsson, M.B., Öquist M., Järveoja J., Peichl M .(2019) .A Novel Approach for High-Frequency in-situ Quantification of Methane Oxidation in Peatlands. Soil Systems 3: 4

Oksanen, J., Blanchet, F. G., Kindt, R., Oksanen, M. J., & Suggests, M. (2013). Package 'vegan.' Community Ecology Package Version.

Olefeldt, D., Goswami, S., Grosse, G., Hayes, D., Hugelius, G., Kuhry, P., … Turetsky, M. R. (2016). Circumpolar distribution and carbon storage of thermokarst landscapes. Nature Communications, 7, 13043. https://doi.org/10.1038/ncomms13043

Olefeldt, D., Euskirchen, E. S., Harden, J., Kane, E., McGuire, A. D., Waldrop, M. P., & Turetsky, M. R. (2017). A decade of boreal rich fen greenhouse gas fluxes in response to natural and experimental water table variability. Global Change Biology, 23(6), 2428–2440. https://doi.org/10.1111/gcb.13612

Parada, A. E., Needham, D. M., & Fuhrman, J. A. (2016). Every base matters : assessing small subunit rRNA primers for marine microbiomes with mock communities , time series and global field samples. 18, 1403–1414. https://doi.org/10.1111/1462-2920.13023

Pelletier, N., Talbot, J., Olefeldt, D., Turetsky, M., Blodau, C., Sonnentag, O., & Quinton, W. L. (2017). Influence of Holocene permafrost aggradation and thaw on the paleoecology and carbon storage of a peatland complex in northwestern Canada. Holocene, 27(9), 1391–1405. https://doi.org/10.1177/0959683617693899

Perryman, C. R., McCalley, C. K., Malhotra, A., Fahnestock, M. F., Kashi, N. N., Bryce, J. G., … Varner, R. K. (2020). Thaw Transitions and Redox Conditions Drive Methane Oxidation in a Permafrost Peatland. Journal of Geophysical Research: Biogeosciences, 125(3). https://doi.org/10.1029/2019JG005526

Pinheiro J, Bates D, DebRoy S, S. D. and R. C. T. (2017). nlme: Linear and Nonlinear Mixed Effects Models. R package version 3.1-131, https://CRAN.R-project.org/package=nlme. R Package Version 3.1-131, Https://CRAN.R-Project.Org/Package=nlme. https://doi.org/10.1016/j.tibs.2011.05.003

Preuss I, Knoblauch C, Gebert J & Pfeiffer EM (2013) Improved quantification of microbial CH4 oxidation efficiency in arctic wetland soils using carbon isotope fractionation. Biogeosciences 10: 2539-2552

Quince, C., Lanzen, A., Davenport, R. J., & Turnbaugh, P. J. (2011). Removing Noise From Pyrosequenced Amplicons.

R Core Team. (2015). R: A language and environment for statistical computing. Vienna, Austria; 2014. URL Http://Www. R-Project. Org. Vienna, Austria: R Foundation for Statistical Computing. https://doi.org/10.1007/978-3-540-74686-7

Robroek, B. J. M., Jassey, V. E. J., Kox, M. A. R., Berendsen, R. L., Mills, R. T. E., Cécillon, L., … Bodelier, P. L. E. (2015). Peatland vascular plant functional types affect methane dynamics by altering microbial community structure. Journal of Ecology, 103(4). https://doi.org/10.1111/1365-2745.12413

Robroek, B. J. M., Martí, M., Svensson, B. H., Dumont, M. G., Veraart, A. J., & Jassey, V. E. J. (2021). Rewiring of peatland plant–microbe networks outpaces species turnover. Oikos, 130(3). https://doi.org/10.1111/oik.07635

Schaefer, K., Zhang, T., Bruhwiler, L., & Barrett, A. P. (2011). Amount and timing of permafrost carbon release in response to climate warming. Tellus, Series B: Chemical and Physical Meteorology, 63(2). https://doi.org/10.1111/j.1600-0889.2011.00527.x

Schuur, E. A. G., McGuire, A. D., Schädel, C., Grosse, G., Harden, J. W., Hayes, D. J., … Vonk, J. E. (2015). Climate change and the permafrost carbon feedback. Nature, 520(7546), 171–179. https://doi.org/10.1038/nature14338

Simon, E., Canarini, A., Martin, V., Séneca, J., Böckle, T., Reinthaler, D., … Richter, A. (2020). Microbial growth and carbon use efficiency show seasonal responses in a multifactorial climate change experiment. Communications Biology, 3(1). https://doi.org/10.1038/s42003-020-01317-1

Strack, M., Waddington, J. M., & Tuittila, E. S. (2004). Effect of water table drawdown on northern peatland methane dynamics: Implications for climate change. Global Biogeochemical Cycles. https://doi.org/10.1029/2003GB002209

Stams A.J.M., Teusink B., Sousa D.Z. (2019) Ecophysiology of Acetoclastic Methanogens. In: Stams A., Sousa D. (eds) Biogenesis of Hydrocarbons. Handbook of Hydrocarbon and Lipid Microbiology. Springer, Cham. https://doi.org/10.1007/978-3-319-78108-2_21

1278 Strom, L., Falk, J.M., Skov, K., Jackowizc-Korczynski, M., Mastepanov, M., Christensen, T.,
1279 Lund, M., Schmidt, N.M. (2015). Controls of spatial and temporal variabilirt in CH4 flux in a
1280 high arctic fen over three years. Biogeochemistry 125(1): 21-35.
1281 Treat, C. C., & Jones, M. C. (2018). Near-surface permafrost aggradation in Northern
1282 Hemisphere peatlands shows regional and global trends during the past 6000 years.
1283 Holocene. https://doi.org/10.1177/0959683617752858
1284
1285 Turetsky, M. R., Wieder, R. K., Vitt, D. H., Evans, R. J., & Scott, K. D. (2007). The
1286 disappearance of relict permafrost in boreal north America: Effects on peatland carbon
1287 storage and fluxes. Global Change Biology, 13(9), 1922–1934.
1288 https://doi.org/10.1111/j.1365-2486.2007.01381.x
1289
1290 Turetsky, Merritt R., Abbott, B. W., Jones, M. C., Anthony, K. W., Olefeldt, D., Schuur, E.
1291 A. G., … McGuire, A. D. (2020). Carbon release through abrupt permafrost thaw.
1292 Nature Geoscience. https://doi.org/10.1038/s41561-019-0526-0
1293
1294 Tuittila, E. S., Komulainen, V. M., Vasander, H., Nykanen, H., Martikainen, P. J., & Laine, J.
1295 (2000). Methane dynamics of a restored cut-away peatland. Global Change Biology, 6(5),
1296 569–581. https://doi.org/10.1046/j.1365-2486.2000.00341.x
1297
1298 Vitt, D. H., Halsey, L. A., Bauer, I. E., & Campbell, C. (2000). Spatial and temporal trends in
1299 carbon storage of peatlands of continental western Canada through the Holocene.
1300 Canadian Journal of Earth Sciences, 37(5), 683–693. https://doi.org/10.1139/e99-097
1301
1302 Vitt, D. H., Halsey, L. A., & Zoltai, S. C. (1994). The Bog Landforms of Continental Western
1303 Canada in Relation to Climate and Permafrost Patterns. Arctic and Alpine Research,
1304 26(1), 1. https://doi.org/10.2307/1551870
1305
1306 Weishaar, J.L., Aiken, G.R., Bergamaschi, B.A., Fram, M.S., Fujii, R., Mopper, K. (2003).
1307 Evaluation of specific ultraviolet absorbance as an indicator of the chemical composition and
1308 reactivity of dissolved organic carbon. Environmental Science and Technology 37(20): 4702-
1309 4708. https://doi.org/10.1021/es030360x
1310
1311 Whiticar, M. J., Faber, E., & Schoell, M. (1986). Biogenic methane formation in marine and
1312 freshwater environments: CO2 reduction vs. acetate fermentation-Isotope evidence.
1313 Geochimica et Cosmochimica Acta, 50(5). https://doi.org/10.1016/0016-7037(86)90346-
1314 7
1315
1316 Whiticar, Michael J. (1999). Carbon and hydrogen isotope systematics of bacterial formation
1317 and oxidation of methane. Chemical Geology, 161(1). https://doi.org/10.1016/S0009-
1318 2541(99)00092-3
1319
1320 Wickham, H. (2016). ggplot2 -Positioning Elegant Graphics for Data Analysis. In Springer.
1321

https://doi.org/10.5194/bg-2021-337
Preprint. Discussion started: 11 January 2022


Biogeosciences
Discussions
Open Access
EGU

Wickland, K. P., Striegl, R. G., Neff, J. C., & Sachs, T. (2006). Effects of permafrost melting on CO2 and CH4 exchange of a poorly drained black spruce lowland. Journal of Geophysical Research: Biogeosciences, 111(2), 1–13. https://doi.org/10.1029/2005JG000099

Ye, R., Jin, Q., Bohannan, B., Keller, J. K., McAllister, S. A., & Bridgham, S. D. (2012). PH controls over anaerobic carbon mineralization, the efficiency of methane production, and methanogenic pathways in peatlands across an ombrotrophic-minerotrophic gradient. Soil Biology and Biochemistry, 54, 36–47. https://doi.org/10.1016/j.soilbio.2012.05.015

Zoltai, S. C. (1972). Palsas and Peat Plateaus in Central Manitoba and Saskatchewan. Canadian Journal of Forest Research, 2(3), 291–302. https://doi.org/10.1139/x72-046

Zoltai, S. C. (1993). Cyclic Development of Permafrost in the Peatlands of Northwestern Alberta, Canada. Arctic and Alpine Research, 25(3), 240. https://doi.org/10.2307/1551820